Charged Silicon Nitride Films: Field-Effect Passivation of Silicon Solar Cells and a Novel Characterization Method through Lifetime Measurements

by

Qun Yang

A Thesis Presented in Partial Fulfillment
of the Requirements for the Degree
Master of Science

Approved April 2014 by the
Graduate Supervisory Committee:

Stuart Bowden, Chair
Christiana Honsberg
Clarence Tracy

ARIZONA STATE UNIVERSITY

May 2014

ABSTRACT

Silicon (Si) solar cells are the dominant technology used in the Photovoltaics industry. Field-effect passivation by means of electrostatic charges stored in an overlying insulator on a silicon solar cell has been proven to be a significantly efficient way to reduce effective surface recombination velocity and increase minority carrier lifetime. Silicon nitride (SiN_x) films have been extensively used as passivation layers. The capability to store charges makes SiN_x a promising material for excellent feild effect passivation.

In this work, symmetrical $Si/SiO_2/SiN_x$ stacks are developed to study the effect of charges in SiN_x films. SiO_2 films work as barrier layers. Corona charging technique showed the ability to inject charges into the SiN_x films in a short time. Minority carrier lifetimes of the Czochralski (CZ) Si wafers increased significantly after either positive or negative charging.

A fast and contactless method to characterize the charged overlying insulators on Si wafer through lifetime measurements is proposed and studied in this work, to overcome the drawbacks of capacitance–voltage (CV) measurements such as time consuming, induction of contanmination and hysteresis effect, etc. Analytical simulations showed behaviors of inverse lifetime (Auger corrected) vs. minority carrier density curves depend on insulator charge densities (N_f). From the curve behavior, the Si surface condition and region of N_f can be estimated.

When the silicon surface is at high strong inversion or high accumulation, insulator charge density (N_f) or surface recombination velocity parameters (S_{n0} and S_{p0}) can be determined from the slope of inverse lifetime curves, if the other variable is

known. If S_{n0} and S_{p0} are unknown, N_f values of different samples can be compared as long as all have similar S_{n0} and S_{p0} values. Using the saturation current density (J_0) and intercept fit extracted from the lifetime measurement, the bulk lifetime can be calculated. Therefore, this method is feasible and promising for charged insulator characterization.

ACKNOWLEDGMENTS

I would like to express my great appreciation to Dr. Stuart Bowden for providing me the opportunity to research under his supervision. I am grateful to him for providing me guidance and resources on my research. His encouragement has led me to overcome one challenge after another. I am also grateful to Dr. Clarence Tracy for his outstanding guidance and numerable hours of discussion. I was so influenced by his unfathomable knowledge on the semiconductor. I am thankful to Dr. Christiana Honsberg for providing me with useful ideas during my research period. She is the director of quantum energy and sustainable solar technologies (QESST) engineering research center. Thank her for providing me with a great resource of solar research and network.

I am thankful to Bill Dauksher for his training on the cleanroom and guidance on many lab tools. I would like to thank Dr. Kunal Ghosh for his excellent discussion with me. I would like to extend my thanks to Dr. James Hwang at Amtech Systems, Inc. for the discussion on silicon nitride charging.

I would also like to thank my friends and colleagues at ASU Solar Power Lab (SPL). It has been a wonderful time to working with them and I am happy to spend nearly two years with them at SPL.

Finally, I wish to thank all my family members and friends for their support and understanding during the three years of graduate study and research.

TABLE OF CONTENTS

Page

CHAPTER Page

LIST OF TABLES

Table Page

LIST OF FIGURES

Figure Page

Figure Page

Figure Page

CHAPTER 1

INTRODUCITON

1.1 Energy Revolution through Photovoltaics

Energy required in the modern world is mainly generated from fossil fuels for a long period of time [1]. However, the use of fossil fuels has led to increased emission of greenhouse gases which is the main reason for global warming over the past 50 years [2]. Renewable energy is the energy generated from sustainable sources such as water, sunlight, etc. Renewable energy is environmentally friendly and has little greenhouse gas emission during the generation process.

Photovoltaics (PV) is one of the most promising types of renewable energy. PV is a direct way to convert sunlight to electric power though devices called solar cells. The forecast of the energy use is shown in Fig. 1.1. The use of solar power is expected to be growing rapidly in the following decades and be the dominant energy source by 2100. The rapid growth of PV actually took place from 2000, as shown in Fig. 1.2. The PV market was driven by Europe, especially Germany, before 2012. Then in 2013, the global market is more driven by other countries such as China, US, Japan, etc. Now the use of solar power keeps growing in many places around the world and is expected to dominate energy revolution in the future.

A solar cell is a semiconductor device that can generate electrical current when it is under illumination. Electron-hole pairs in a semiconductor can be generated via absorption of light. Photogenerated electrons and holes move randomly resulting in zero current flow if they are not driven to a specific direction. The formation of a p-n junction

in a semiconductor device is the typical way to force electrons to move in a certain direction while holes move in the opposite direction, thus creating current flow.

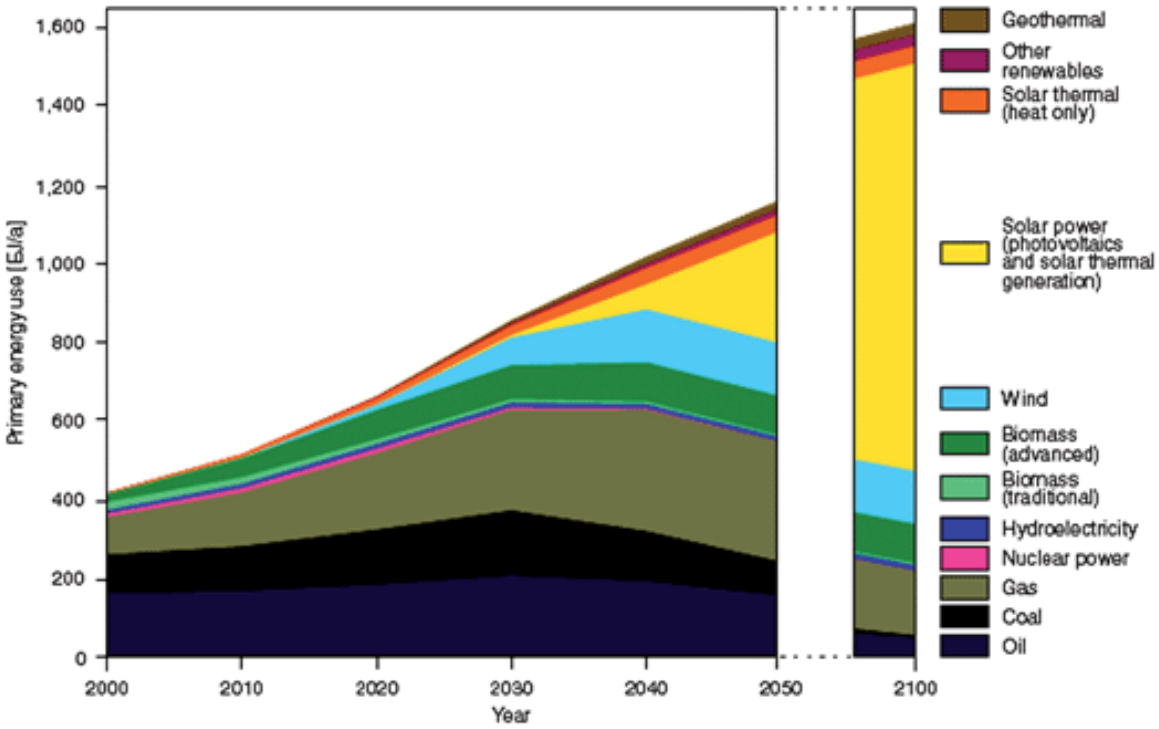

Fig. 1.1. Forecast of the energy use by different sources until 2050/2100 [3].

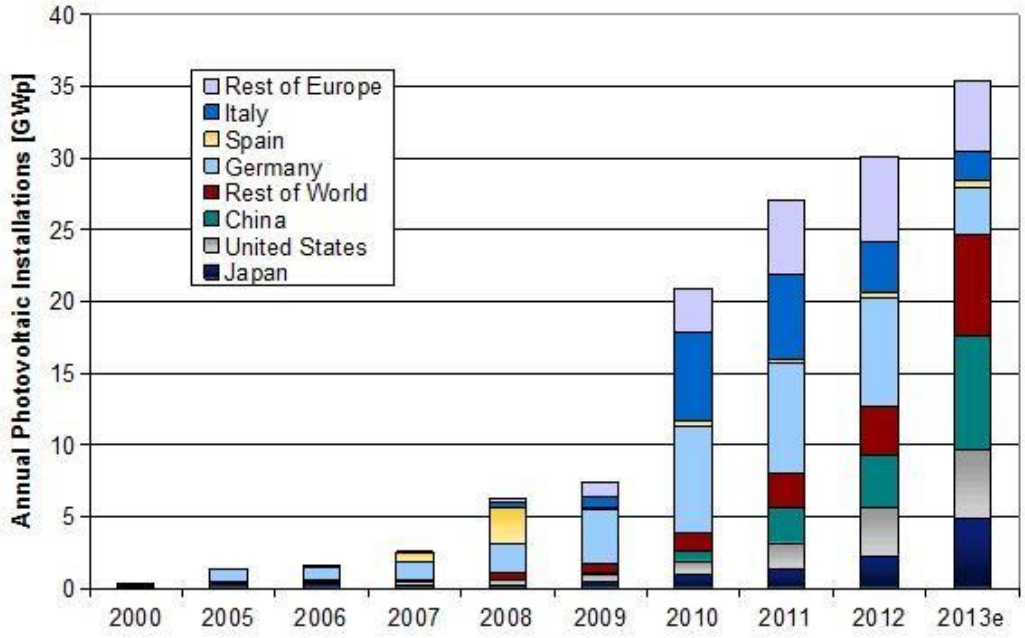

Fig. 1.2. Global annual PV installations from 2000 to 2013 [4].

1.2 Motivation for this Work

Crystalline silicon (c-Si) solar cells, including mono and multi-crystalline silicon solar cells, have been the major technology used in the industry for many years, as shown in Fig. 1.3. Therefore, improving performance and reducing cost of c-Si solar cells are important for increasing the use of solar power.

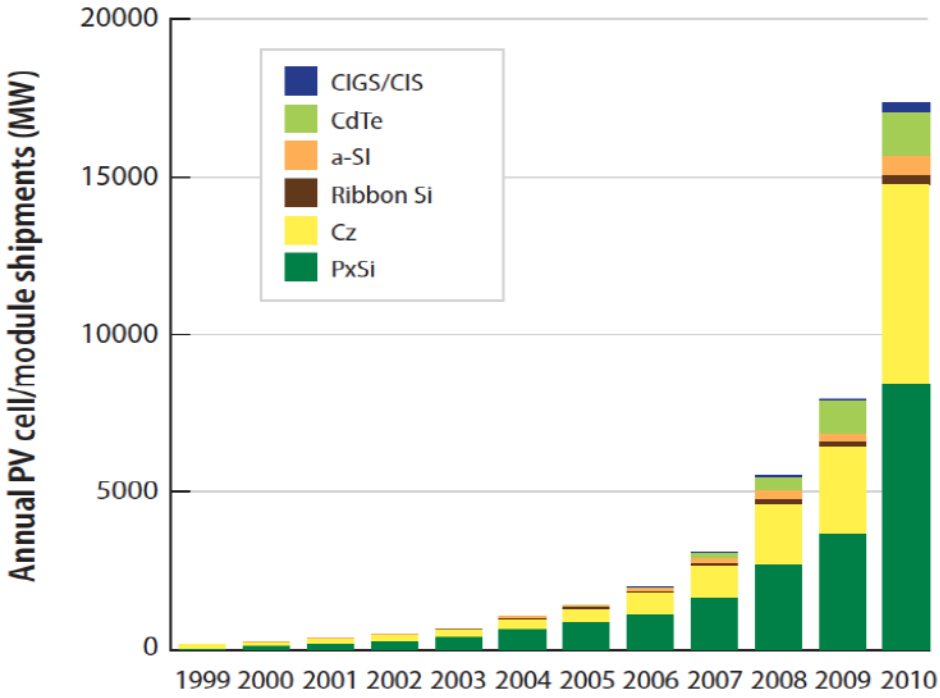

Fig. 1.3. Global annual PV cell and module shipments by PV technology [5].

Surface passivation is a crucial technique for the c-Si solar cells. The aim of surface passivation is to reduce surface recombination velocity and improve minority carrier lifetime. Chemical passivation and field-effect passivation are two effective ways for surface passivation. Field-effect passivation by means of electrostatic charges in an overlying insulator on a silicon solar cell has been proven to be a significantly efficient way to increase minority carrier lifetime [6], [7]. Silicon Nitride (SiN_x) films are

commonly used as the surface passivation layer. The ability of SiN_x films to store charges of either polarity makes SiN_x a promising material for excellent field-effect passivation.

This thesis studies the mechanism of charges stored in the SiN_x films, and its effect on minority carrier lifetime. Additionally, a novel method to characterize the overlying insulator through lifetime measurement is proposed and studied, to overcome the disadvantages of traditional capacitance–voltage (CV) measurement. CV measurement is extensively used to find out the charge density in the insulating film on the semiconductor. However, CV measurement is timing consuming compared to lifetime measurement, and is unable to be integrated in a solar cell pilot line. Due to the hysteresis effect in CV measurements, it is difficult to get stable experimental CV curves. The distribution of charges in either as-deposited or corona charged SiN_x films has poor uniformity, which makes it hard to get a reliable result from single CV measurement.

CHAPTER 2

RECOMBINATION MECHANISM AND SURFACE CONDITION

2.1 Bulk Recombination

Recombination of an electron and a hole is a major type of loss in solar cells. The minority carrier lifetime (τ) is a function of injection level (Δn) and recombination rate (U), given by

$$\tau \equiv \frac{\Delta n}{U} \tag{2.1}$$

Recombination loss reduces both the short-circuit current via the current collection and the open-circuit voltage via the forward bias diffusion current [8]. In solar cells, recombination happens both in the bulk (referred to as *bulk recombination*) and at the surface (referred to as *surface recombination*). Bulk recombination consists of three recombination processes: radiative recombination, Auger recombination and Shockley-Read-Hall (SRH) recombination.

2.1.1 Radiative recombination

Radiative recombination is the direct band-to-band recombination of an electron and a hole, where an electron in the conduction band drops down to the valence band and radiates a photon. Radiative recombination is a major recombination mechanism in the direct band semiconductor. The radiative recombination rate (U_{rad}) is given by

$$U_{rad} = Bnp = B(n_0 + \Delta n)(p_0 + \Delta n) \tag{2.2}$$

where B is the radiative recombination coefficient, n and p are electron and hole concentrations, n_0 and p_0 are the carrier concentrations at equilibrium, and Δn and Δp are

the excess carrier densities under illumination. The value of B is 9.5×10^{-15} for silicon [9]. From Equations (2.1) and (2.2), the radiative lifetime is given by

$$\tau_{rad} = \frac{\Delta n}{B(n_0 + \Delta n)(p_0 + \Delta n)} \tag{2.3}$$

2.1.2 Auger recombination

Auger recombination is a band-to-band recombination of an electron and a hole with exiting a third electron or hole to a higher energy level. Auger recombination is a combination of the two-electron (and one-hole) process and the two-hole (and one-electron) process. The total recombination rate U_{Auger} is given by

$$U_{Auger} = C_n n^2 p + C_p n p^2 \tag{2.4}$$

where C_n and C_p are Auger coefficients of two-electron process and two-hole process, respectively. Low injection condition is defined as excess carrier density Δn is much (10x) less than doping concentration, while high injection is condition defined as Δn is much (10x) higher than doping concentration. Auger lifetimes are

$$\tau_{Auger,high} = \frac{1}{C_n N_D^{\,2}} \qquad \text{(n-type)} \tag{2.5a}$$

$$\tau_{Auger,low} = \frac{1}{C_p N_A^{\,2}} \qquad \text{(p-type)} \tag{2.5b}$$

$$\tau_{Auger,high} = \frac{1}{(C_n + C_p)\Delta n^2} \qquad \text{(both n-type and p-type Si)} \tag{2.6}$$

For Silicon, the most commonly used auger coefficients are those determined by Dziewior and Schmid: $C_n = 2.8 \times 10^{-31}$ cm^6/s and $C_p = 9.9 \times 10^{-32}$ cm^6/s [10]. Those values are valid for dopant concentration higher than 5×10^{18} cm^{-3}. Auger recombination becomes a major process with high background doping concentration or at high injection.

2.1.3 Shockley-Read-Hall recombination

Shockley-Read-Hall (SRH) recombination is a process in which an electron and a hole recombine via defects in the semiconductor. “Defects” (or “traps”) introduced by impurities and dislocations create additional energy levels between the conduction and valence bands. Those energy levels increase the recombination probability by splitting a single large step as in the radiative recombination into two steps with much lower excitation energy needed. The recombination rate via single-level defect is given by the model independently developed by Shockley and Read, and Hall [11], [12]

$$U = \frac{np - n_i^2}{\tau_{p0}(n + n_1) + \tau_{n0}(p + p_1)} \tag{2.7}$$

with

$$\tau_{n0} = \frac{1}{\sigma_n N_t \nu_{th}} \qquad \tau_{p0} = \frac{1}{\sigma_n N_t \nu_{th}} \tag{2.8}$$

$$n_1 = n_i \, exp(\frac{E_t - E_i}{kT}) \qquad p_1 = n_i \, exp(\frac{E_i - E_t}{kT}) \tag{2.9}$$

where τ_{n0} and τ_{p0} are the electron and hole lifetimes, which are determined by the capture cross section for electrons (σ_n) and holes (σ_p), the trap density (N_t), and the thermal velocity (ν_{th}), n_1 and p_1 are related to the intrinsic carrier concentration (n_i), the trap energy level (E_t), the intrinsic energy level (E_i), and the temperature (T). k is the Boltzmann constant.

From Equations (2.1) and (2.7), the SRH lifetime is given by

$$\tau_{SRH} = \frac{\tau_{p0}(n + n_1) + \tau_{n0}(p + p_1)}{n_0 + p_0 + \Delta n} \tag{2.10}$$

The relationship between τ_{SRH} and Δn is shown in Fig. 2.1. At either low or high injection, τ_{SRH} is constant and τ_{SRH} is higher at high injection; at mid-injection, τ_{SRH} is

injection level dependent. The SRH recombination is the dominant process in indirect band semiconductors, such as silicon, under low injection.

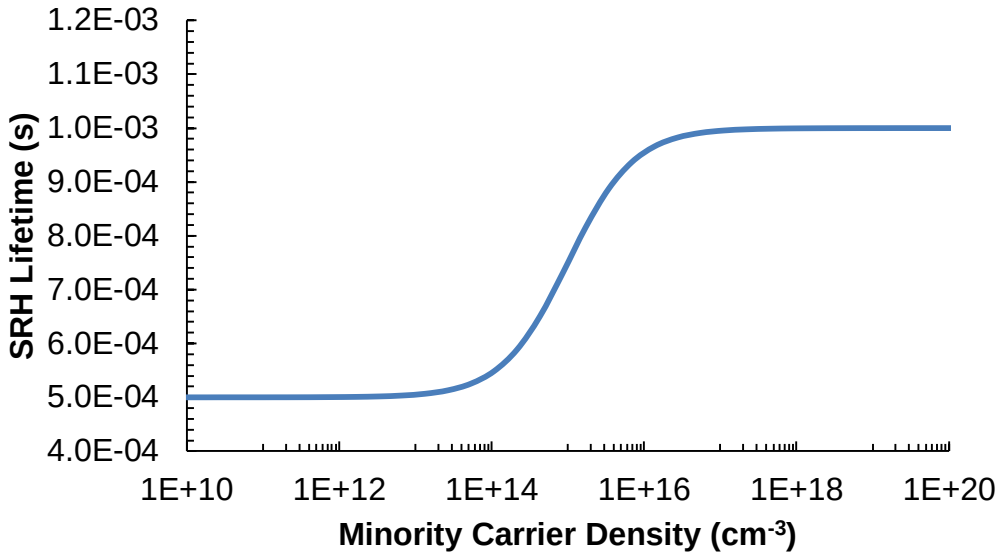

Fig. 2.1. Dependence of SRH lifetime on injection level, for n-type Si with doping concentration of $1x10^{15}$ cm^{-3}, $\tau_{n0}=\tau_{p0}=$ 0.5 ms, single-level defects at midgap.

Bulk lifetime including each constituent with respect to the injection level is shown in Fig. 2.2. This simulation is performed using an online simulation tool at *PV Lighthouse* [13]. The recombination models used are: Schlangenotto 1974 for radiative recombination; Dziewior-Schmid 1977 for Auger recombination; SRH equation (with $\tau_{n0}=\tau_{p0}=$500 μs, single-level defect at midgap) for SRH recombination. When the silicon wafer is at low injection, SRH recombination plays a major role. As the injection level is increasing, Auger recombination becomes more and more important. Radiative recombination is not the dominant process at any injection level; it is thus neglected for analytical simulations in CHAPTER 4.

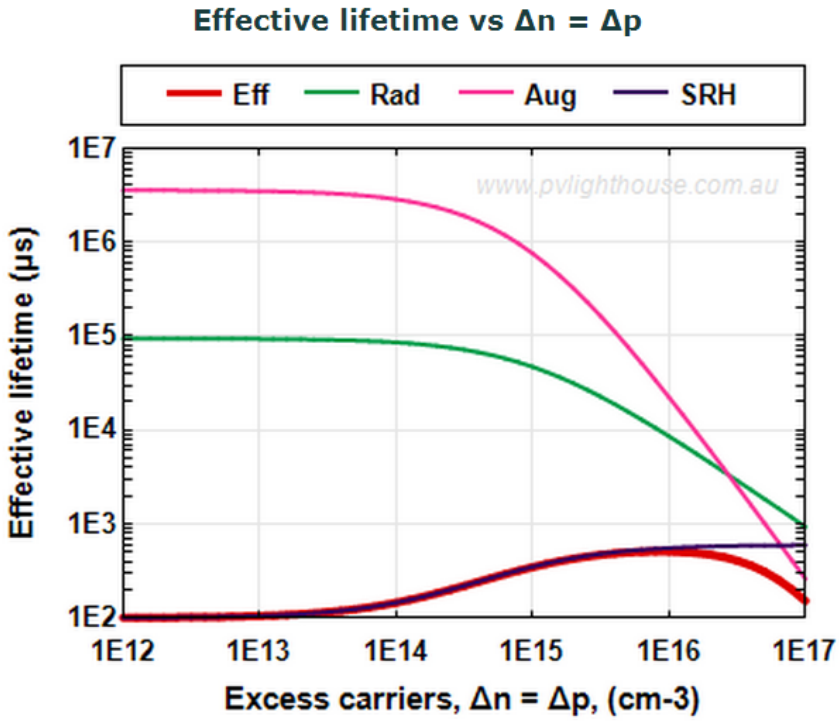

Fig. 2.2. Theoretical dependence of bulk lifetime and its constituents on the injection level, for n-type Si with doping concentration of $1x10^{15}$ cm^{-3}.

2.2 Semiconductor Surface

2.2.1 Energy-band diagram of MIS

To study charged insulating films, a metal-insulator-semiconductor (MIS) capacitor is the basic structure to begin with. A standard screen-printed c-Si solar cell has a MIS capacitor at the front surface, consisting of a silicon emitter, a silicon nitride (SiN_x) layer as anti-reflection coating, and silver metal contact.

The following discussion is based on Sze's book [14]. The energy-band diagram of an ideal MIS structure with no applied bias is shown in Fig. 2.3. For an ideal MIS structure, there is no charge in the insulator or carrier transport through the insulator. The symbols used in Fig. 2.3 are explained in Table 2.1. ϕ_{ms} is the work function difference between metal and semiconductor, which is given by

$$\phi_{ms} \equiv \phi_m - \phi_s = \phi_m - (\chi - \phi_n) \qquad \text{(n-type)} \qquad (2.11a)$$

$$\phi_{ms} \equiv \phi_m - \phi_s = \phi_m - (\chi + \frac{E_g}{q} - \phi_p) \qquad \text{(p-type)} \qquad (2.11b)$$

The bands are flat for in the semiconductor and the insulator, which is described as the *flat-band* condition.

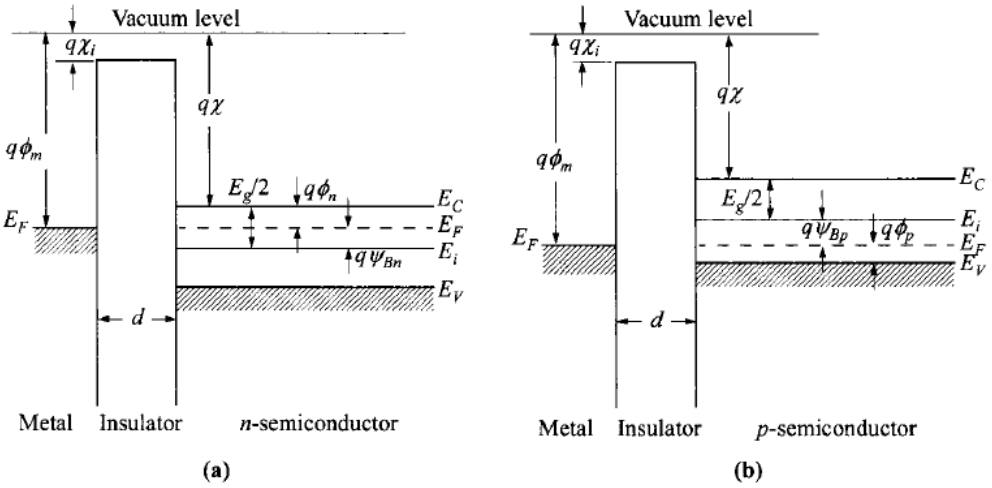

Fig. 2.3. Energy-band diagrams of ideal MIS capacitors at equilibrium of (a) n-type semiconductor, (b) p-type semiconductor [14].

When there are charges present in the overlying insulator, there is energy-band bending near the surface, as shown in Fig. 2.4. There is no current flow for an ideal structure, which means $dE_F/dx=0$, so the Fermi level is flat. When there are positive charges in the insulator, the bands near the surface bend downward and the electrons (majority carriers) are accumulated, resulting in the *accumulation* condition. When there is a small amount of negative charges in the insulator, the bands near the surface bend upward and the electrons are depleted, resulting in the *depletion* condition. When the density of negative insulator charges is high enough to bend bands upward to a certain

level so that E_i is higher than E_F at the surface, the concentration of holes (minority carriers) is higher than that of electrons, resulting in the *inversion* condition.

Table 2.1. Symbols used in Fig. 2.3.

Symbol	Description	Unit
q	Elementary charge, = 1.6×10^{-19} C, absolute value	C
χ	Electron affinity (for semiconductor)	V
χi	Electron affinity for insulator	V
ϕ_m	Metal work function	V
ϕ_s	Semiconductor function, potential difference between vacuum level and Fermi level	V
D	Thickness of insulator	cm
E_g	Band gap between the conduction and valence bands	eV
ψ_{Bn}	Fermi level from intrinsic Fermi level in n-type material, $=\|E_F - E_i\|/q$	V
ψ_{Bp}	Fermi level from intrinsic Fermi level in p-type material, $=\|E_F - E_i\|/q$	V
ϕ_n	Potential difference from conduction band edge to Fermi level, $=(E_C - E_F)/q$	V
ϕ_p	Potential difference from Fermi level to valence band edge, $=(E_F - E_V)/q$	V

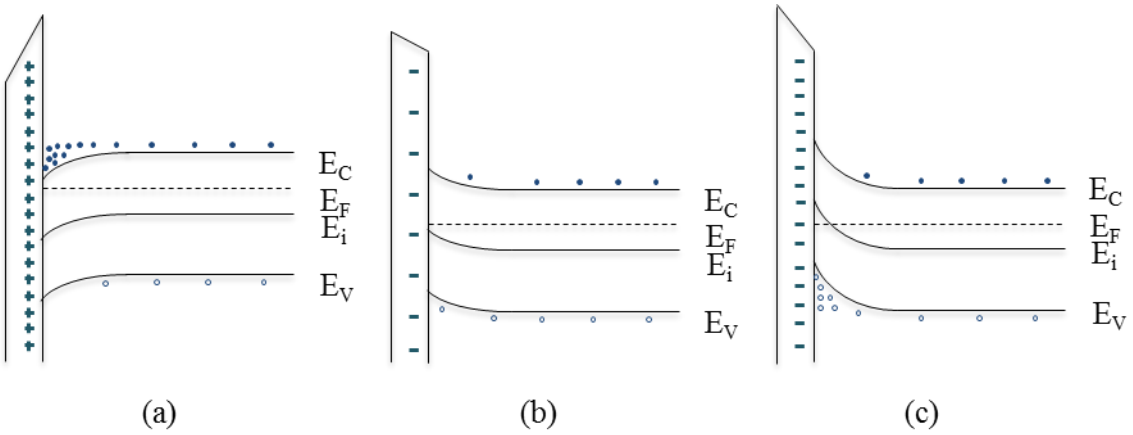

Fig. 2.4. Energy-band diagrams of n-type semiconductor with different charges in the overlying insulator, for the conditions of (a) accumulation, (b) depletion and (c) inversion.

In the p-type semiconductor, holes are the majority carriers. For each surface condition, the polarity of insulator charges is opposite to that on the n-type semiconductor. Thus negative insulator charges create the accumulated surface, while positive insulator charges create the depleted or inverted surface.

2.2.2 Surface space-charge density at equilibrium

Fig. 2.5 shows a more detailed energy-band diagram of an n-type semiconductor surface at inversion. ψ_n is the potential at n-type semiconductor boundary with respect to the bulk, and it is given by

$$\psi_n(x) \equiv -\frac{[E_i(x) - E_i(\infty)]}{q} \tag{2.12}$$

where $E_i(\infty)$ is intrinsic Fermi level in the bulk. Note that ψ_n is positive when bands bend downward. At the semiconductor surface ($x=0$), $\psi_n(0)$ is denoted as ψ_s (surface potential). ψ_{net} and ψ_{inv} are discussed in Section 4.4.1.Then the electron and hole concentrations can be expressed as

$$n_n(x) = n_{n0}\, exp\left(\frac{q\psi_n}{kT}\right) = n_{n0}\, exp(\beta\psi_n) \tag{2.13a}$$

$$p_n(x) = n_{n0}\, exp\left(-\frac{q\psi_n}{kT}\right) = n_{n0}\, exp(-\beta\psi_n) \tag{2.13b}$$

with
$$\beta = \frac{q}{kT} \tag{2.14}$$

where n_{n0} and p_{n0} are the electron and hole concentrations at equilibrium . The electron and hole concentrations at the surface (n_s and p_s) are then given by

$$n_s = n_{n0}\, exp(\beta\psi_s) \tag{2.15a}$$

$$p_n = n_{n0}\, exp(-\beta\psi_s) \tag{2.15b}$$

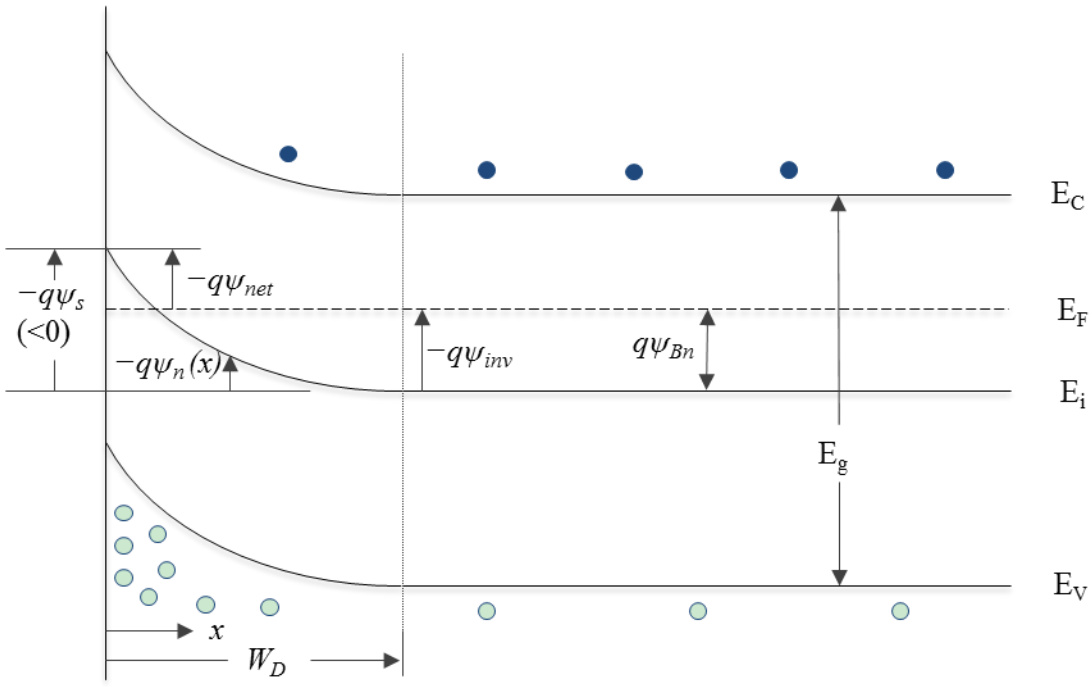

Fig. 2.5. Detailed energy-band diagram of an n-type semiconductor with an inverted surface.

Poisson equation gives the relationship between potential ψ_n and space charge density ρ

$$\frac{d^2\psi_n}{dx^2} = -\frac{\rho(x)}{\varepsilon_s} \tag{2.16}$$

with
$$\rho(x) = q(N_D^+ - N_A^- + p_n - n_n) \tag{2.17}$$

The bulk of the semiconductor is electrically neutral, thus

$$N_D^+ - N_A^- = n_{n0} - p_{n0} \tag{2.18}$$

Therefore Equation (2.16) becomes

$$\begin{aligned}\frac{d^2\psi_n}{dx^2} &= -\frac{q}{\varepsilon_s}(n_{n0} - p_{n0} + p_n - n_n) \\ &= -\frac{q}{\varepsilon_s}\{p_{n0}[exp(-\beta\psi_n) - 1] - n_{n0}[exp(\beta\psi_n) - 1]\}\end{aligned} \tag{2.19}$$

Electric field (E) can be obtained by integrating Equation (2.19)

$$E^2 = \left(\frac{2}{\beta}\right)^2 \left(\frac{qn_{n0}\beta}{2\varepsilon_s}\right)\left\{\frac{p_{n0}}{n_{n0}}[exp(-\beta\psi_n) + \beta\psi_n - 1] + [exp(\beta\psi_n) - \beta\psi_n - 1]\right\} \tag{2.20}$$

The following abbreviations can be used

$$L_{Dn} \equiv \sqrt{\frac{\varepsilon_s}{qn_{n0}\beta}} \equiv \sqrt{\frac{kT\varepsilon_s}{q^2 n_{n0}}} \tag{2.21}$$

$$F\left(\beta\psi_n, \frac{p_{n0}}{n_{n0}}\right) \equiv \sqrt{\frac{p_{n0}}{n_{n0}}[exp(-\beta\psi_n) + \beta\psi_n - 1] + [exp(\beta\psi_n) - \beta\psi_n - 1]} \tag{2.22}$$

with
$$\frac{p_{n0}}{n_{n0}} = exp(-2\beta\psi_{Bn}) \tag{2.23}$$

where L_{Dn} is extrinsic Debye length for electrons. We can then express the electric field as

$$E(x) = \pm \frac{\sqrt{2}kT}{qL_{Dn}} F\left(\beta\psi_n, \frac{p_{n0}}{n_{n0}}\right) \tag{2.24}$$

$$E_s = \pm \frac{\sqrt{2}kT}{qL_{Dn}} F\left(\beta\psi_s, \frac{p_{n0}}{n_{n0}}\right) \tag{2.25}$$

where E_s is the electric field at the semiconductor surface ($x=0$). E is positive for $\psi_n>0$ and negative for $\psi_n<0$. According to Gauss's law, total space charge per unit area near the n-type semiconductor surface is given by

$$Q_s = -\varepsilon_s E_s = \mp \frac{\sqrt{2}\varepsilon_s kT}{qL_{Dn}} F\left(\beta\psi_s, \frac{p_{n0}}{n_{n0}}\right) = \mp \frac{\sqrt{2}\varepsilon_s}{\beta L_{Dn}} F\left(\beta\psi_s, \frac{p_{n0}}{n_{n0}}\right) \tag{2.26}$$

That means Q_s is a function of ψ_s for a given semiconductor material. For the n-type semiconductor with $\psi_s>0$, surface is in the accumulation condition, and Q_s is negative; when $\psi_s=0$, surface is in the flat-band condition and Q_s is zero; when $\psi_s<0$, the surface is in the depletion or inversion condition, and Q_s is positive. Fig. 2.6 shows the relationship between the space-charge density, surface concentrations of electrons and holes at equilibrium ($n_{s,\,eqb}$ and $p_{s,\,eqb}$) and the surface potential. Note that the y-axis is the absolute value of Q_s/q.

In CHAPTER 4, a novel characterization method using lifetime measurement is proposed and discussed. The analytical simulation is performed using n-type silicon substrate with the doping concentration of $1x10^{15}$ cm^{-3}, which gives a ψ_{Bn} value of 0.298 V. The excess carrier density (Δn) in the lifetime measurement is typically less than $1x10^{17}$ cm^{-3}. For the purpose of simulation results analysis, surface conditions are further defined based on the traditional way in this work. *Low* and *high* (accumulation or strong inversion) are distinguished by the surface carrier concentration of $1x10^{18}$ cm^{-3} at equilibrium due to band bending, which is 10x higher than the upper limit of Δn in the

simulation. The relationship between the surface condition and insulator charge density (N_f) is shown in Table 2.2 and Fig. 2.6.

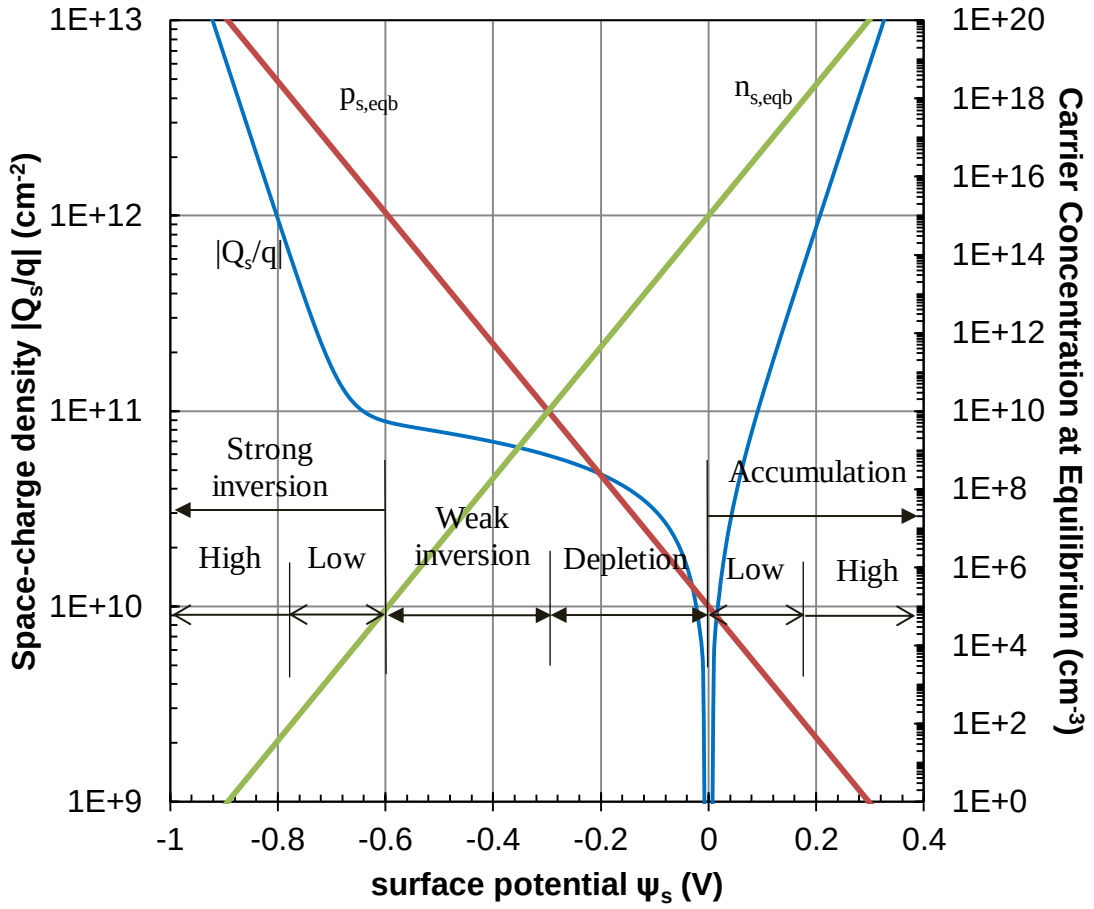

Fig. 2.6. Illustration of $|Q_s/q|$, $n_{s,eqb}$ and $p_{s,eqb}$ as a function of surface potential ψ_s for n-type silicon with doping concentration of $1x10^{15}cm^{-3}$.

The slight difference between $|Q_f/q|$ value at high accumulation and high strong inversion is because this is an n-type semiconductor. There are slightly less charges required to achieve $n_{s,eqb}=1x10^{18}$ cm^{-3} than $p_{s,eqb}=1x10^{18}$ cm^{-3}.

Table 2.2. Relationship of surface condition, surface potential and insulator charge density. For n-type silicon with the doping concentration of $1x10^{15}$ cm^{-3}.

Surface condition	**Surface potential (V)**	**Insulator charge density (cm^{-2})**
High accumulation	$\psi_s > 0.179$	$Q_f/q > +5.8x10^{11}$
Low accumulation	$0.179 > \psi_s > 0$	$+5.8x10^{11} > Q_f/q > 0$
Flat-band	$\psi_s = 0$	$Q_f/q = 0$
Depletion	$-0.298 < \psi_s < 0$	$-5.9x10^{10} < Q_f/q < 0$
Fermi-level at midgap	$\psi_s = -0.298$	$Q_f/q = -5.9x10^{10}$
Weak inversion	$-0.596 < \psi_s < -0.298$	$-8.8x10^{10} < Q_f/q < -5.9x10^{10}$
Low strong inversion	$-0.774 < \psi_s < -0.596$	$-5.9x10^{11} < Q_f/q < -8.8x10^{10}$
High strong inversion	$\psi_s < -0.774$	$Q_f/q < -5.9x10^{11}$

2.3 Surface Recombination

A Si atom has four valence electrons and each requires one valence electron from another Si atom to be paired. At the silicon surface, there are not enough atoms to make all valence electrons paired. The unpaired electrons are commonly referred to as *dangling bonds*, as shown in Fig. 2.7. Dangling bonds create a large density of defects (surface states) between the conduction and valence band. Each surface state acts as a SRH recombination center, resulting in significantly high recombination probability, as shown in Fig. 2.8. Described by the SRH theory Equation (2.7), the surface recombination rate U_s via single-level state is expressed as

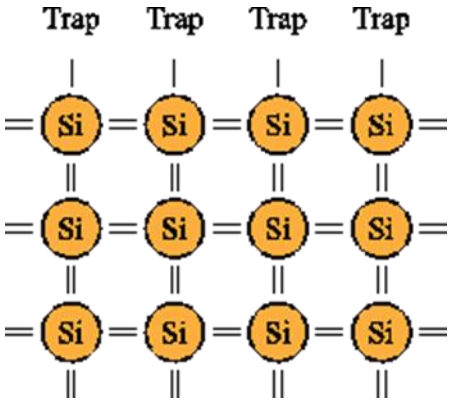

Fig. 2.7. Illustration of dangling bonds at silicon surface [15].

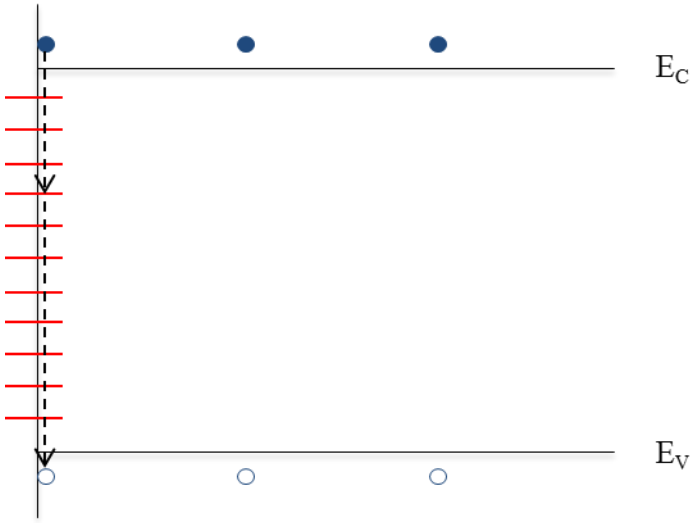

Fig. 2.8. Energy band diagram illustrating recombination via surface states.

$$U_s = \frac{n_s p_s - n_i^2}{\frac{n_s + n_1}{S_{p0}} + \frac{p_s + p_1}{S_{n0}}} \tag{2.27}$$

with $S_{n0} = \sigma_n N_{st} \nu_{th}$ $S_{p0} = \sigma_n N_{st} \nu_{th}$ (2.28)

where n_s and p_s are the electron and hole concentrations at the surface, S_{n0} and S_{p0} are the surface recombination velocity parameters of electrons and holes, and N_{st} is the surface state (trap) density. Note that U_s is in unit of $cm^{-2}s^{-1}$ not $cm^{-3}s^{-1}$ as the bulk recombination rate U, and N_{st} is in unit of cm^{-2}. S_{n0}, S_{p0} are in unit of $cm \cdot s^{-1}$, which is the same as

velocity. When the semiconductor contains a large amount of surface states at various energy levels, U_s can be described as

$$U_s = \int_{E_V}^{E_C} \frac{n_s p_s - n_i^2}{\frac{n_s + n_1}{\sigma_p(E)} + \frac{p_s + p_1}{\sigma_n(E)}} v_{it} D_{it}(E) dE \tag{2.29}$$

where D_{it} is the surface state density per unit energy (cm^{-2}/eV), and E_C and E_V are the conduction and valence band energy levels, respectively. Integration of D_{it} from E_C to E_V is used to substitute N_{st} for single-level state.

The surface recombination velocity (SRV) S is defined as

$$S \equiv \frac{U_s}{\Delta n_s} \tag{2.30}$$

2.3.1 Flat-band condition at the surface

When the semiconductor surface is in the flat-band condition, the excess concentrations of electrons (Δn_s) and holes (Δp_s) are equal under illumination. Then we can use Δn_s to represent the excess carrier concentration at the surface. Note that Δn_s is constant in the semiconductor from the bulk to the surface, as the energy bands are flat. By substituting Equation (2.27) into (2.30) , the SRV becomes

$$S = \frac{n_0 + p_0 + \Delta n_s}{\frac{n_0 + n_1 + \Delta n_s}{S_{p0}} + \frac{p_0 + p_1 + \Delta n_s}{S_{n0}}} \tag{2.31}$$

According to the above equation, surface recombination velocity is a function of SRV parameters, injection level and doping concentration. By referring to Equations (2.9) and (2.28), SRV parameters are determined by energy level of traps (E_t), trap density (N_{st}) and capture cross sections for electrons (σ_n) and holes (σ_p).

The SRV is independent of Δn_s at low or high injections. For the n-type semiconductor under low injection, we can assume that $n_0 >> \Delta n_s >> p_0$, and $n_1, p_1 >> \Delta n_s$. Then Equation (2.31) becomes

$$S_{low} = \frac{S_{p0}}{1 + \frac{1}{n_0}\left(n_1 + p_1 \frac{S_{p0}}{S_{n0}}\right)} \tag{2.32}$$

For the p-type semiconductor, there is an analogous relationship. So the SRV at low level injection depends on the energy level of traps (E_t), and the SRV parameters (S_{n0}, S_{p0}). Thus S_{low} is irrelevant to injection level.

Under high injection, we can assume that $\Delta n_s >> n_0 >> p_0$, and $\Delta n_s >> n_1, p_1$ for the n-type semiconductor. Then Equation (2.31) becomes

$$S_{high} = \frac{S_{p0}}{1 + \frac{S_{p0}}{S_{n0}}} \tag{2.33}$$

This shows S_{high} is a constant for given S_{n0} and S_{p0}.

2.3.2 Surface band bending condition

For the MIS structure, the energy-bands at the semiconductor surface are usually not flat, due to the charges in the insulator and non-zero metal-semiconductor work function difference. In this case, Δn_s and Δp_s are not equal under illumination. Thus there is no analytical expression for the SRV. An effective SRV (S_{eff}) is then used alternatively and defined as [16]

$$S_{eff} = \frac{U_s}{\Delta n(x = d)} \tag{2.34}$$

S_{eff} is in terms of Δn at the edge of space charge region ($x=d$) instead of Δn_s (at the surface). The variable d is measured from the surface. As the energy bands are flat in the quasi-neutral region, Δn ($x=d$) is the excess carrier concentration in the bulk.

In the dark, the effective SRV is a function of $n_{s,eqb}$ and $q_{s,eqb}$ (eqb means at equilibrium), which are determined by the surface potential, as shown in Fig. 2.9. The maximum S_{eff} occurs at -0.298 V where $n_{s,eqb}=q_{s,eqb}$ (the Fermi-level at midgap, referring to Table 2.2). S_{eff} decreases significantly with either higher $n_{s,eqb}$ (accumulation) or higher $p_{s,eqb}$ (strong inversion). Therefore, a high lifetime in the Si solar cell can be obtained through bending the surface bands to a high level.

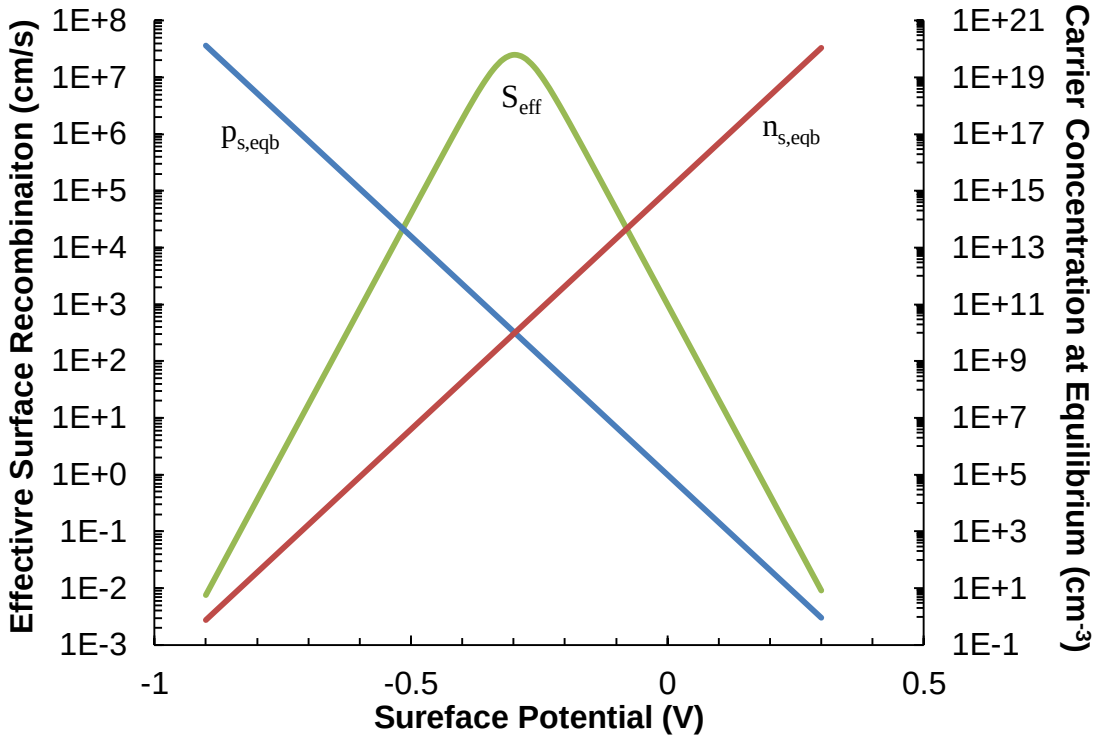

Fig. 2.9. Effect of surface potential and surface carrier concentration on effective SRV in the dark. Simulation parameters: $n_0=1x10^{15}$ cm^{-3}, $S_{n0}=S_{p0}=1000$ cm/s, single-level defect at midgap.

CHAPTER 3

FIELD-EFFECT PASSIVIATION

3.1 Surface Passivation

There are two approaches to reduce surface recombination velocity [16]: (a) optimization of the surface property to reduce surface state density (D_{it}), and (b) reduction of surface concentrations of electrons and holes.

3.1.1 Optimization of the surface property to reduce surface state density

This approach is by film deposition or growth (usually silicon oxide or silicon nitride) on the Si substrate. The formation of electron pairs between Si and passivating film reduces unpaired electrons at the bare Si surface dramatically, resulting in a much lower amount of Si surface dangling bonds. In this way, D_{it} decreases to a very low level. For example, interface state density (N_{it}) for non-passivated Si is of the order of $1x10^{-13}$ cm^{-2}, while N_{it} for oxide passivated Si can be as low as $1x10^{-9}$ cm^{-2} [16]. According to Equations (2.31) and (2.29), a low D_{it} value leads to a low surface recombination rate. This approach is called *chemical passivation*.

After thermal oxidation, *hydrogen passivation* can be performed to further reduce D_{it}. A common hydrogen passivation method is annealing the overlying oxide film in forming gas (a mixture of N_2 and H_2), which is called forming gas anneal (FGA). A more effective method is evaporating aluminum (Al) on the oxide before FGA, which is usually referred to as *alneal* [17].

3.1.2 Reduction of surface concentrations of electrons and holes

According to Fig. 2.9, the maximum S_{eff} occurs where $n_{s,eqb}=p_{s,eqb}$. S_{eff} decreases with either higher $n_{s,eqb}$ or higher $q_{s,eqb}$. This phenomenon can be explained physically through the recombination process. When the concentration of one type of carrier is higher than it is at equilibrium, the concentration of the other type of carrier must be lower, according to $n_{s,eqb}\,p_{s,eqb} = n_i^2$. The recombination rate is limited by the lower carrier concentration, because both an electron and a hole are required during the recombination process. When $n_{s,eqb}$ and $q_{s,eqb}$ are equal, S_{eff} reaches its maximum.

There are usually two methods to achieve the reduction of surface concentration of one type of carrier:

a) formation of a higher doping region near the silicon surface;

b) field-effect passivation.

One example of the first method is back surface field (BSF) in c-Si solar cells. BSF is formed by a high-low junction (p^+p or n^+n). For p-type silicon solar cells, a common way to create the p^+p junction is firing screen-printed Al (back contact) into Si, creating a p^+ region at the back surface, where Al atoms work as p-type dopants.

The second method, field-effect passivation, is achieved by charges stored in the overlying film (dielectric layer). Charges create band bending near the Si surface, resulting in a different surface condition. When the surface is at accumulation or strong inversion, the surface concentration of dominant carriers at equilibrium is higher than that at flat-band condition, leading to a much smaller S_{eff}.

The most investigated insulators for c-Si solar cells are gown thermal silicon oxide and plasma-enhanced chemical vapor deposited (PECVD) silicon nitride [16]. Both

films hold as-deposited positive fixed charges, which create an accumulated surface for an n-type emitter and reduce the SRV effectively. Their charge properties are discussed in the following section.

3.2 Charges in the Insulator

3.2.1 Charges in the silicon oxide

There are four types of charges associated with thermal silicon oxide: fixed charges (Q_f), interface-trapped charges (Q_{it}), oxide trapped charges (Q_{ot}) and mobile ionic charges (Q_m), as shown in Fig. 3.1. All terms Q_f, Q_{it}, Q_{ot}, and Q_m are charge densities in unit of C/cm^{-2} and are discussed as below [14], [16], [18], [19]:

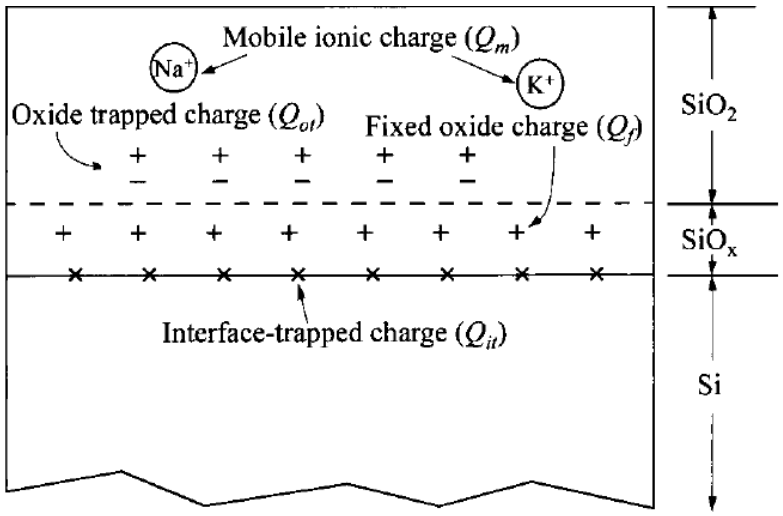

Fig. 3.1. Illustration of charges associated with thermal silicon oxide [14].

i) Q_f locates in the oxide where it is very close ($\leq$ 2 nm) to the Si/SiO_2 interface. Q_f cannot be changed by a gate voltage or illumination. A corresponding term N_f (in unit of cm^{-2}) describes the number of elementary charges per area, which is denoted as $N_f \equiv Q_f/q$. A thermal oxide usually has an N_f value of $5x10^{10}$–$2x10^{11}$ cm^{-2}. Unlike Q_{it} or Q_{ot}, Q_f is constant and cannot be affected by illumination or anneal.

b) Q_{it} is the density of charges trapped by interface states within the bandgap. Interface states above a neutral energy level (E_0) are acceptor-like, which means they are negatively charged when occupied by an electron and neutral when unoccupied. Accordingly, interface states below E_0 are acceptor-like, which means they are positive charged when occupied by a hole and neutral when unoccupied. These behaviors of interface states show the opposite way of bulk defects. Q_{it} can be significantly reduced via hydrogen passivation like forming gas anneal (FGA). D_{it} is used as interface state density per unit energy (cm^{-2}/eV) and the relationship between D_{it} and Q_{it} is

$$Q_{it} = -q\int_{E_0}^{E_F} D_{it}\,dE \qquad (E_F \text{ above } E_0) \qquad (3.1a)$$

$$Q_{it} = q\int_{E_0}^{E_F} D_{it}\,dE \qquad (E_F \text{ below } E_0) \qquad (3.1b)$$

c) Q_m is the density of mobile charges inside the oxide, which is due to ionic impurities such as Na^+, Li^+, and K^+. Q_m can almost be neglected in modern technique with proper wafer and furnace cleaning.

d) Q_{ot} may be caused by electrons or holes trapped in the oxide. Q_{ot} can be reduced by the anneal process.

In this work, the device used has two insulator layers: SiO_2 layer and SiN_x layer. Total insulator charge density is described as N_f to represent all charges in SiO_2 and SiN_x.

3.2.2 Charge property of silicon nitride film

Silicon nitride deposited by chemical vapor deposition (CVD, including PECVD) method is non-stoichiometric amorphous silicon nitride with up to 40 % hydrogen [16]. This type of silicon nitride is denoted as a-SiN_x: H, and abbreviated as SiN_x in this work.

Silicon nitride was first studied in the metal/nitride/semiconductor (MNS) and metal/nitride/oxide/semiconductor (MNOS) structures used in memory devices [20]-[22]. Hysteresis characteristics were observed for both the MNS and the MNOS structures, indicating the existence of defects (traps) exist in the SiN_x. Electron spin resonance (ESR) approaches showed that the dominant defects (traps) in SiN_x are Si dangling bonds. For each Si atom, three valence electrons are paired with valence electrons of N atom, leaving one unpaired electron in the Si atom to form a dangling bond ($N_3{\equiv}Si\cdot$). This Si dangling bond becomes a trap center, which is usually referred to as the K center [23]-[26]. The K center defects are amphoteric traps which means they can trap either electrons or holes, as shown in Fig. 3.2. Therefore, the silicon nitride film is able to store charges of either polarity via K centers. There exist three types of states for K centers depending on the electron occupation status: K^0 (neutral, one electron), K^+ (positive, no electron) and K^- (negative, two electrons). The total density of K centers is finite and the percentage of each type of states can be detected by ESR measurements [27]-[29].

However, for the Si/SiN_x structure, the fixed charges (N_f) in SiN_x are very unstable. Because charges can tunnel through Si/SiN_x interface easily due to the Poole-Frenkel effect, the SiN_x film cannot hold a large amount of charges [20]-[22]. For the purpose of characterization of charge density in the SiN_x film, a stable Q_f value over time and during measurement is required. In this work, a layer of silicon oxide is used between the SiN_x film and the Si substrate as a barrier, to prevent charge transport. The insulator is a thermal-SiO_2/PECVD-SiN_x stack, as shown in Fig. 3.3.

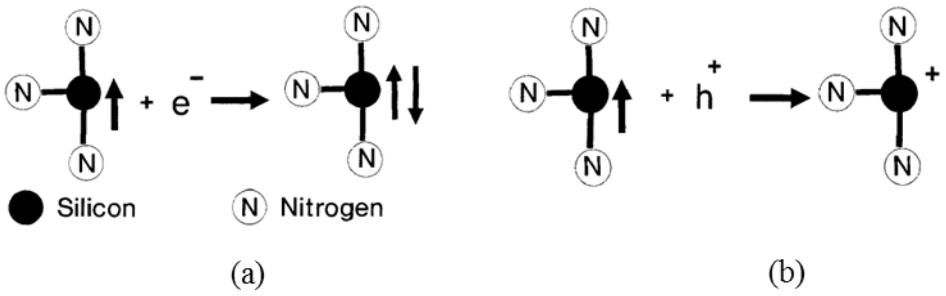

Fig. 3.2. Demonstration of the neutral K center (K^0) trapping (a) an electron (K^-), (b) a hole (K^+) [30].

3.3 Sample Fabrication

Samples used in this work were prepared at Arizona State University (ASU) Solar Power Lab. The wafers used were 3-inch Czochralski (CZ) grown n-type (phosphorus doped) silicon substrate with a <100> surface crystal orientation. They were double-side polished with resistivity of 1-10 Ω-cm (~ $1x10^{15}$ cm^{-3}). Symmetrical $Si/SiO_2/SiN_x$ stacks were developed as shown in Fig. 3.3.

Fabrication procedure of this device is shown in Table 3.1. Wet chemical cleaning with three solutions was the first procedure and it is an important way of chemical passivation of Si surface. Piranha solution is a mixture of sulfuric acid (H_2SO_4) and hydrogen peroxide (H_2O_2) with a ratio of 4:1. The purpose of piranha etch is to remove organic residues off the wafers. RCA is short for a company name "Radio Corporation of America". RCA-B solution is a mixture of deionized water, hydrochloric acid (HCl) and hydrogen peroxide (H_2O_2) with a ratio of 5:1:1. The purpose of RCA-B clean is to eliminate metallic (ionic) contamination. BOE is the abbreviation for buffered oxide etch, which is used to remove silicon oxide.

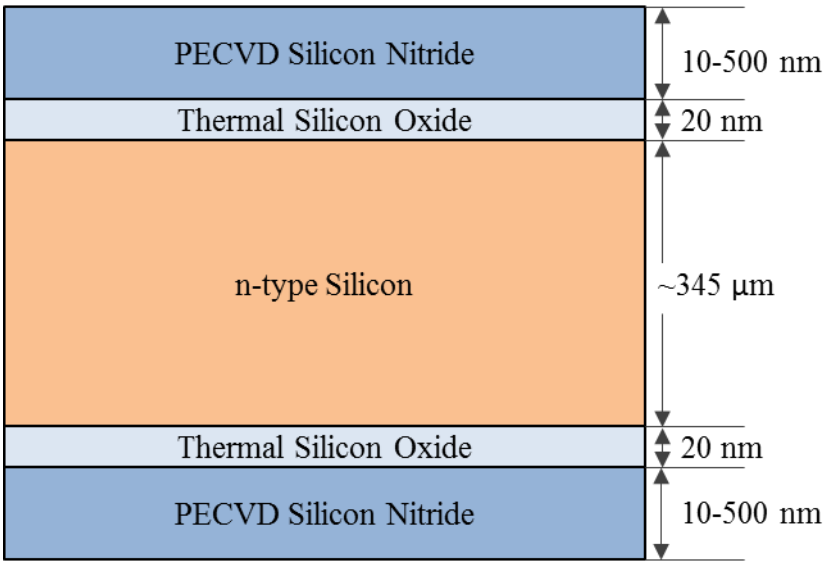

Fig. 3.3. Schematic diagram of the symmetrical $Si/SiO_2/SiN_x$ stack used in this work.

Table 3.1. Fabrication procedure of the charged symmetrical $Si/SiO_2/SiN_x$ stack.

Order	Procedure	Details
1	Cleaning	10 min Piranha, 10 min RCA-B, 2 min BOE
2	Thermal oxidation	1100 ℃ Dry oxidation, 20 nm film
3	FGA	400 ℃
4	PECVD SiN_x deposition	200 ℃, 10–500 nm film
5	FGA	400 ℃
6	Corona charging	1 min

After wafer cleaning, SiO_2 films were grown on both sides by dry thermal oxidation. The dangling bonds at Si surface were well passivated by SiO_2. Samples were then annealed by forming gas to reduce Si/SiO_2 interface states and oxide trapped charges in the films. SiN_x films were deposited on the top of SiO_2 films by PECVD, and the

thickness of SiN_x films is shown in Table 3.2. After another FGA run, charges with either polarity were injected into SiN_x films by corona charging technique.

Table 3.2. Thickness of silicon nitride film of samples used in this work.

Lot	DI0188			DI0206		
Wafer	01	02	03	02	03	04
Thickness (nm)	90	178	460	10	20	40

3.4 Capacitance-Voltage Measurement

The capacitance-voltage (CV) measurement is routinely used to determine the charge density in the insulator for MOS structure. Normalized CV curves for MOS structure are shown in Fig. 3.4. Low-frequency and high-frequency describe the small AC signal applied on the sweeping DC voltage, while deep depletion occurs with a fast DC sweep rate. At low-frequency, this capacitance for n-type substrate is the slope of $|Q_s/q|$ curve in Fig. 2.6. When the surface is in the inversion condition, the curves are different for different voltage sweep conditions. At low-frequency, the recombination-generation rate of minority carriers in the inversion layer can follow the small signal variation. At high-frequency, the recombination-generation rate of minority carriers in the inversion layer cannot follow the frequency and thus the charge exchange occurs in the edge of depletion region. At deep depletion, the sweeping ramp is so fast that the semiconductor surface is unable to come to equilibrium [14].

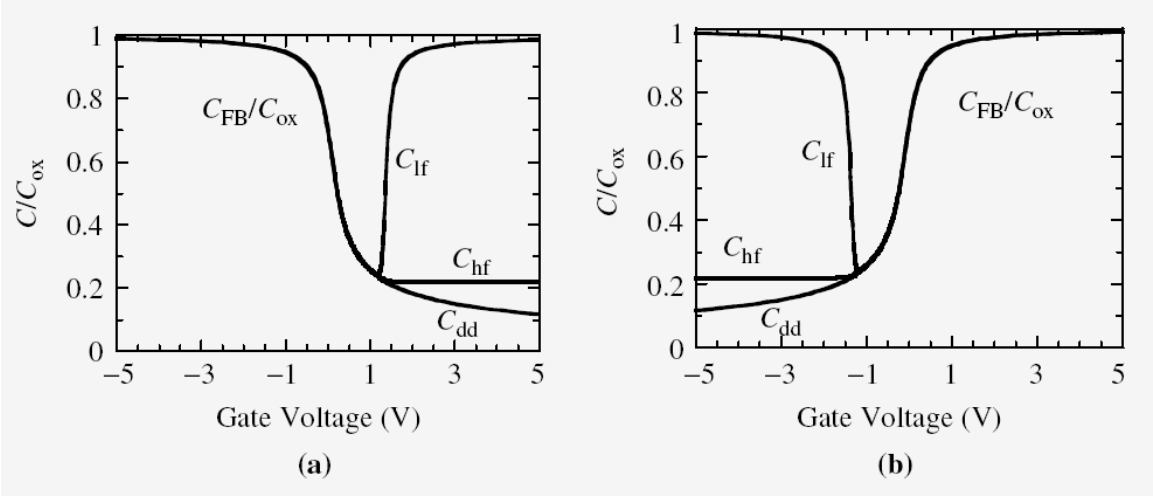

Fig. 3.4. Illustrations of normalized MOS CV curves at low-frequency (lf), high-frequency (hf), and deep-depletion (dd) for (a) p-type substrate and (b) n-type substrate [18].

The relationship between flat-band voltage, metal-semiconductor work function difference, and insulator charges are given by [18]

$$V_{FB} = \phi_{ms} - \frac{Q_f}{C_i} - \frac{Q_{it}(\phi_s)}{C_i} - \frac{1}{C_i}\int_0^{t_i} \frac{x}{t_i}\rho_{ot}(x)\,dx - \frac{1}{C_i}\int_0^{t_i} \frac{x}{t_i}\rho_m(x)\,dx \qquad (3.2)$$

where ρ(x) is the charge per unit volume at distance x, C_i is the capacitance of the insulator and t_i is the thickness of the insulator. When there are charges present in the insulating film, the V_{FB} changes to another value. From the V_{FB} shift with respect to the ideal MIS, insulator charge density can be determined. In this work, charges determined by the CV measurement are simplified as equivalent charges located very close to the Si/SiO_2 interface and the charge density is described as N_f.

To measure CV curve for an insulator-semiconductor structure, metal contacts are required. Aluminum (Al) is a decent material with stable work function as a metal contact. Al contact can be deposited by thermal evaporation, electron beam evaporation or sputtering. However, all these methods are time-consuming due to the high vacuum

process environment. An alternative way is to use mercury (Hg) dot as metal contact. Hg contact is easy to form at room temperature through a mercury probe which is connected to the CV tool. However, there is also a disadvantage for the Hg contact: the work function of Hg as MIS contact is not stable [31]. It gives a large error in the measured N_f when the V_{FB} shift is small. Due to the fact that contamination may be induced for Hg contacts and Al contacts are permanent contacts, it is almost impossible to integrate the CV measurement to determine charge density in a Si solar cell pilot line.

To overcome these disadvantages of the CV measurement, a novel method to determine insulator charge density through lifetime measurement is proposed in CHAPTER 4.

3.5 Corona Charging

Charge injection in the SiN_x film is performed by corona charging technique. A custom-built corona discharge tool is used for the charging experiments. The schematic illustration of the corona charging technique is shown in Fig. 3.5. A copper wire is used as an electrode and the chunk is grounded. The high voltage applied in the electrode can be as high as +/−25,000 V, while the operating voltage is usually 5k-10k V. For the positive applied voltage, positive corona ions (mainly H_3O^+, hydrated protons) are generated and repelled to the surface of SiN_x film due to the electric field between the electrode and chunk. Similarly, for the negative voltage, negative corona ions (mostly CO^{3-}) are generated and repelled to the film surface [32]. Depending on the polarity and time of the applied voltage, the charge polarity and density in the SiN_x film can be changed via K centers, as explained in Section 3.2.

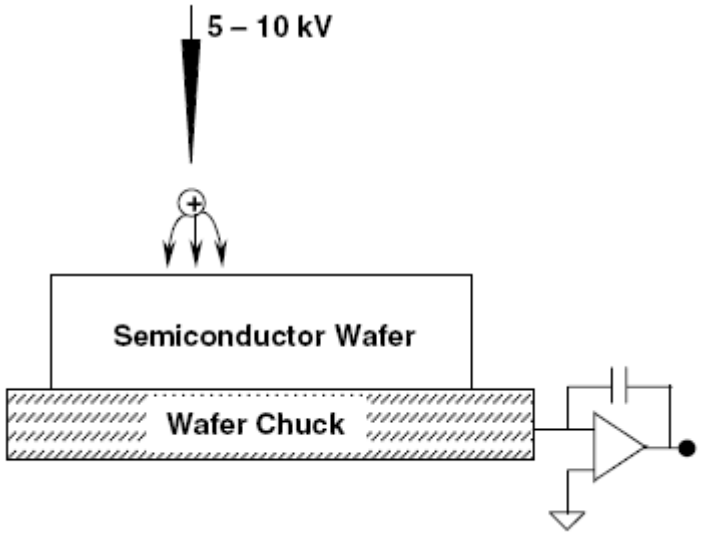

Fig. 3.5. Cross-section schematic of the corona charging technique [32].

The corona charging tool in our lab doesn't have a moving chunk or electrode so the wafer need to be moved manually. To obtain the uniformity of charges, five-point CV measurements around the center of samples were performed before and after negative charging. The charging procedure contains two parts: 1st charging was 30s' charging at the top then move the wafer towards the bottom with an interval of 1 cm; 2nd charging was also 30s' charging but move from left to right with an interval of 1 cm. According to CV curves in Fig. 3.6, negative charges were injected into the SiN_x film after the 1st charging, but with a poor uniformity (26% non-uniformity). After 2nd charging, charge distribution was more uniform (7% non-uniformity). Charges are mostly saturated in the SiN_x film with an average density of -4.2×10^{12} cm^{-2} after 2nd charging, because the maximum flat-band shift is about the same level with that after 1st charging. Therefore the appropriate charging procedure was developed as: 30s charging and moving the wafer with an interval of 1cm from top to bottom then from left to right. In this work, all charging experiments follow this procedure if it is not specified.

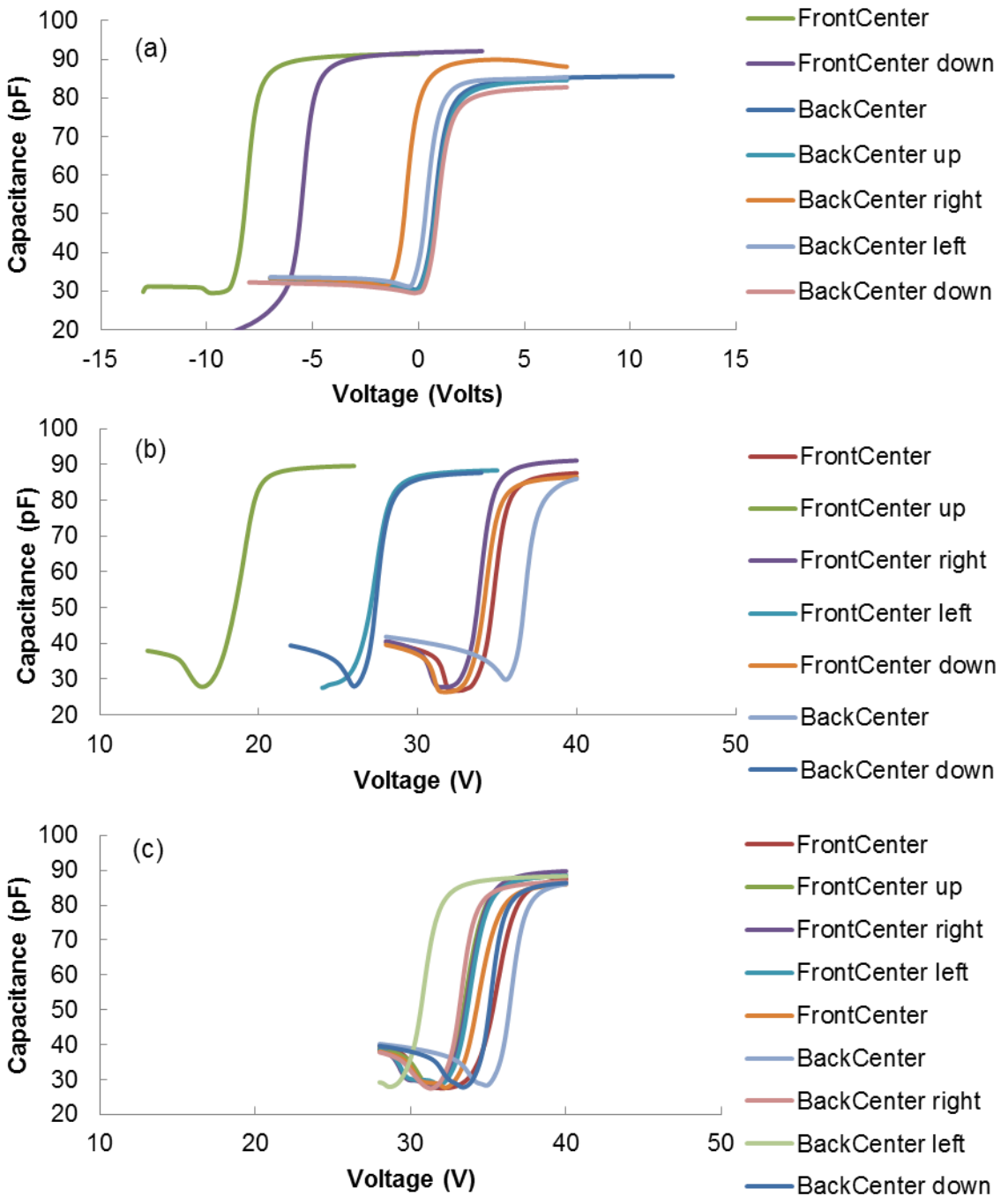

Fig. 3.6. CV curves of wafer DI0188-02 during processes: (a) after FGA, (b) after 1st negative charging, and (c) after 2nd negative charging. Measurements are performed at the center and off the center by 5 mm on both sides.

3.6 Lifetime Improvement

3.6.1 Lifetime measurement introduction

Photoconductance lifetime measurement is extensively used for c-Si solar cells. In this work, the lifetime is measured by *Sinton Instruments WCT-120 photoconductance lifetime tester*, abbreviated as 'lifetime tester'. The measured minority carrier lifetime is commonly referred to as the *effective* lifetime (τ_{eff}), which is determined by bulk recombination and surface recombination [33].

During the measurement, the lifetime tester measures the conductivity (σ) of the wafer from RF coils. The relationship between conductivity and carrier density is given by

$$\sigma = q(n\mu_e + p\mu_h) \tag{3.3}$$

where μ_e and μ_h are electron and hole mobilities, and either is a function of carrier concentration and temperature.

A flash of light is produced from a xenon lamp and passes a 700 nm wavelength infrared (IR) pass filter, generating uniform excess carriers across the wafer. The excess carrier concentration can then be calculated from the difference of measured conductivity after and before flash exposure. The light intensity and generation rate (G) are obtained from a reference solar cell.

There are two analysis methods for different situations: (a) quasi-steady-state photoconductance (QSSPC) decay method [34]; (b) transient photoconductance decay (PCD) method [35]. QSSPC aims to measure a relatively low lifetime (< 200 μs for this lifetime tester) using a long flash exposure time (1s). In this case, the carrier

concentrations are essentially in steady-state, which means the recombination rate (U) and generation rate (G) of carriers are equal. By referring to Equation (2.1), the effective lifetime is then expressed as

$$\tau_{eff} = \frac{\Delta n}{G} \tag{3.4}$$

The transient PCD method aims to measure a relatively high lifetime (>200 μs for this lifetime tester) using a short flash exposure time (1/64 s). In this case, the excess carrier concentrations are not steady, and show an exponential decay with respect to time with the decay time constant (τ_{eff}). The expression is given by

$$\tau_{eff} = \frac{\Delta n}{dn/dt} \tag{3.5}$$

A generalized analysis by recombining the QSSPC and PCD method was proposed by Nagel *et al* [36]. The expression in this case is

$$\tau_{eff} = \frac{\Delta n}{G - dn/dt} \tag{3.6}$$

3.6.2 Experimental lifetime results

As discussed in Section 2.2, S_{eff} drops and minority carrier lifetime τ_{eff} improves significantly for the semiconductor with charged overlying films. From the experimental results, τ_{eff} increased significantly for wafers with either positive or negative corona charged SiN_x films, as shown in Fig. 3.7 and Fig. 3.8. Due to the fact that these wafers are CZ wafers, the bulk time is the upper limit of the total effective lifetime. The low bulk life may be the reason that these lifetimes did not increase dramatically after charging compared to others' experimental results on float-zone (FZ) wafers [6], [37].

Effective lifetimes were measured at the same minority carrier density (MCD) of $7x10^{15}$ cm^{-3} in the following fabrication processes: as-deposited of SiN_x, after FGA of SiN_x, and after negative/positive charging. According to Fig. 3.7, lifetimes increased after both FGA and negative charging. FGA is a hydrogen passivation method, and the charged insulating film provides good field-effect passivation. However, the charging process may create more interface states because of charge transport between the Si substrate and insulator film. The effective lifetime reached to the upper limit due to a low bulk lifetime. The derivation of bulk SRH lifetime will be discussed in Section 4.4.1. The average improvement of lifetime after negative charging for DI0188 was 120% compared to the as-deposited lifetime. Fig. 3.8 shows the lifetime of positive charged samples, also at the MCD of $7x10^{15}$ cm^{-3}. The positive charging resulted in significant improvement of effective lifetime, even compared to that after FGA. The average improvement of effective lifetime after positive charging for DI0206 was 410% compared to the as-deposited lifetime.

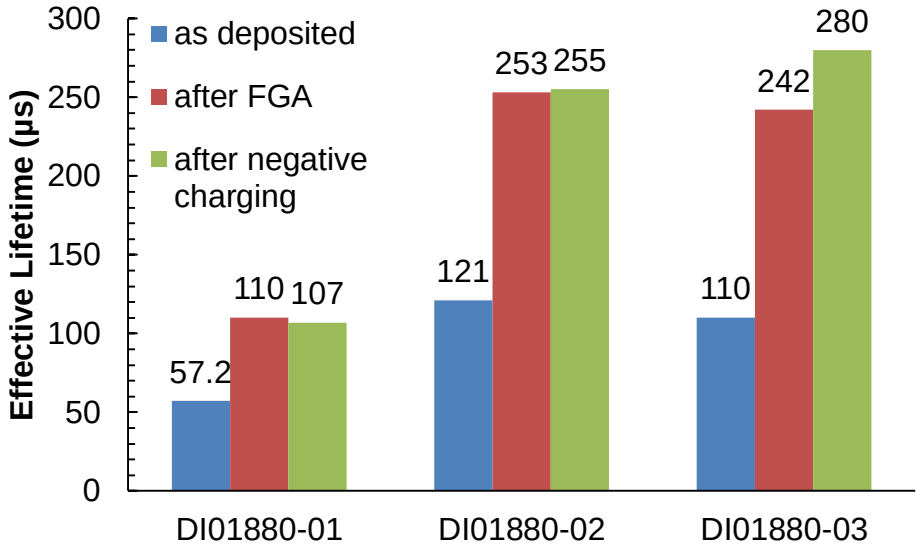

Fig. 3.7. Effect of FGA and negative charges on effective lifetime for symmetrical $Si/SiO_2/SiN_x$ stacks in lot DI0188.

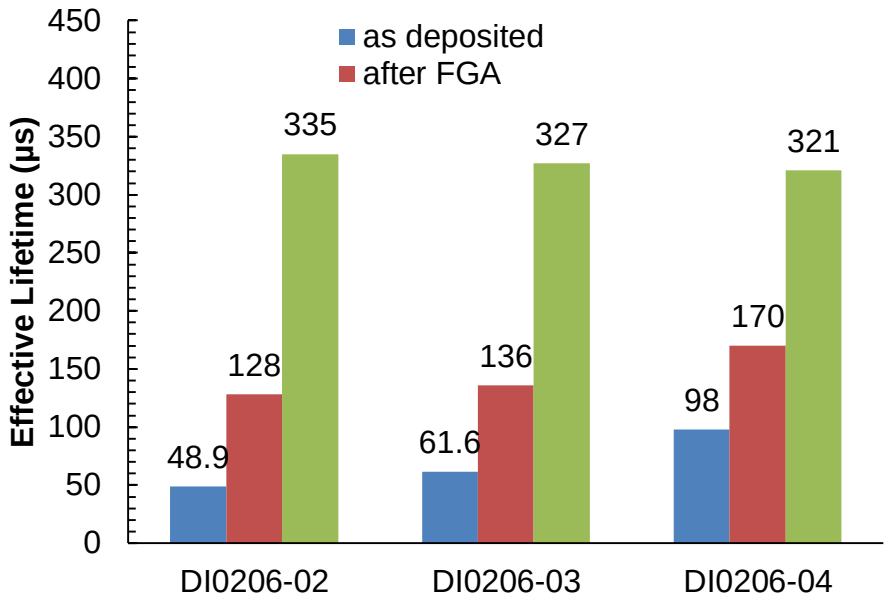

Fig. 3.8. Effect of FGA and positive charges on effective lifetime of symmetrical $Si/SiO_2/SiN_x$ stacks in lot DI0206.

CHAPTER 4

A NOVEL CHARACTERIZATION METHOD THROUGH LIFETIME MEASUREMENTS

4.1 Auger Corrected Inverse Lifetime

The lifetime tester provides another important plot: inverse lifetime (Auger corrected) vs. minority carrier density. From this plot, the saturation current density (J_0) can be extracted. There are several essential conditions to extract the J_0 value: (a) the sample needs to contain a highly-doped region, such as a p-n junction or a high-low junction; (b) extraction should be done in high injection; (c) little generation in the highly-doped region (can be achieved using the IR pass filter); (d) the diffusion length should be much longer than the wafer thickness; (e) the saturation current density is not too high to make transport of carrier limit the recombination rate in the diffused region [33].

Based on the work of Mäckel *et al* [38] and the lifetime tester user manual [33], the equation to extract J_0 is given by

$$\frac{1}{\tau_{eff}} = \frac{1}{\tau_{bulk}} + (J_{0,front} + J_{0,back}) \frac{N_{dop} + \Delta n}{q n_i^2 W} \tag{4.1}$$

where $J_{0,front}$ and $J_{0,back}$ are saturation current densities at the front and rear surface, respectively, and N_{dop} is the background doping concentration. When the IR pass filter is used and the structure is symmetrical, we can assume $J_{0,front}=J_{0,back}=J_0$. Radiative lifetime is insignificant so that it can be neglected. In the lifetime measurement, the Auger corrected inverse lifetime means the impact of Auger recombination has been subtracted out. Thus τ_{bulk} can be considered as containing τ_{SRH} only, which is constant at high

injection. In this work, 'inverse lifetime' is used to represent 'Auger corrected inverse lifetime'. Equation (4.1) can be written as

$$\frac{1}{\tau_{eff}} = \frac{1}{\tau_{bulk}} + \frac{2J_0(N_{dop} + \Delta n)}{qn_i^2 W} \tag{4.2}$$

This shows a linear relationship between $1/\tau_{eff}$ and Δn. J_0 can be extracted from the slope of the linear line. Note that τ_{SRH} is injection dependent for mid-injection. Therefore J_0 should be extracted at high injection to eliminate the effect of τ_{SRH}. In the lifetime measurements, excess carrier densities are usually lower than $5x10^{16}$ cm^{-3}. Thus the Si substrate doping concentration should be sufficiently low (~$1x10^{15}$ cm^{-3}) to ensure accurate extraction of J_0 at high injection.

For a wafer with both well passivated surfaces, the effective minority carrier lifetime is a function of bulk lifetime (τ_{bulk}), effective surface velocity (S_{eff}) and wafer thickness (W), via a simplified relation [16]

$$\frac{1}{\tau_{\text{eff}}} = \frac{1}{\tau_{\text{bulk}}} + \frac{2S_{\text{eff}}}{W} \tag{4.3}$$

Note that Equation (4.3) is valid when both Si surfaces have the same conditions ($S_{eff,front}=S_{eff,back}$). The symmetrical structure used in this work satisfies that requirement.

4.2 Surface Space-Charge Density under Illumination

Solar cells normally work under illumination, in which carriers are not at equilibrium as discussed in the Section 2.2.2. Illumination creates photo-generated carriers in the device, resulting in the steady-state condition.

For the MIS structure under illumination, the energy-band diagrams are shown in Fig. 4.1. Due to photogeneration, electron and hole concentrations are higher than they

are at equilibrium, and can be expressed as functions of quasi-Fermi potentials. Quasi-Fermi potentials for electrons (ϕ_{Fn}) and holes (ϕ_{Fp}) are defined as

$$\phi_{Fn} \equiv -\frac{[E_{Fn} - E_i(\infty)]}{q} \tag{4.4a}$$

$$\phi_{Fp} \equiv -\frac{[E_{Fp} - E_i(\infty)]}{q} \tag{4.4b}$$

where E_{Fn} and E_{Fp} are quasi-Fermi energy levels for electrons and holes, respectively. There is almost no current flow in this structure, which means $dE_{Fn}/dx = 0$, $dE_{Fp}/dx = 0$.

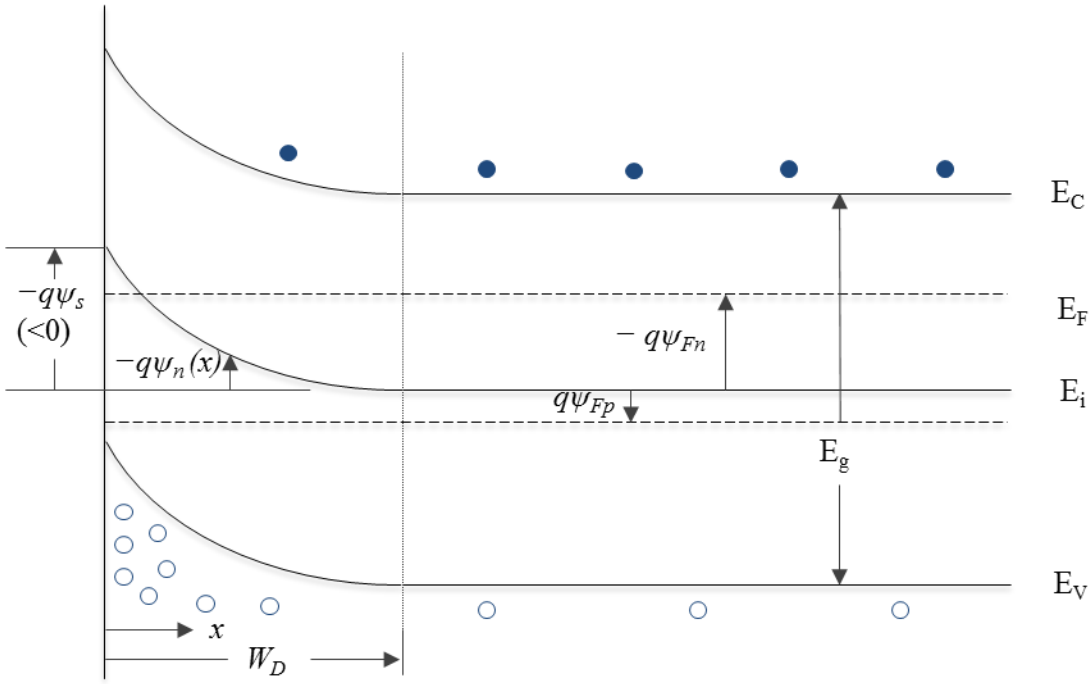

Fig. 4.1. Detailed energy-band diagram of an n-type semiconductor with an inverted surface under illumination.

Thus we can assume quasi-Fermi levels are flat from the semiconductor bulk to surface. The electron and hole concentrations in the bulk are denoted as n(d) and p(d), respectively. n(d) and p(d) are functions of quasi-Fermi potentials

$$n_d = n_i \, exp(-\beta \phi_{Fn}) \tag{4.5a}$$

$$p_d = n_i \, exp(\beta \phi_{Fp}) \tag{4.5b}$$

In the surface space-charge region, electron and hole concentrations are given by

$$n = n_i \, exp[\beta(\psi_n - \phi_{Fn})] \tag{4.6a}$$

$$p = n_i \, exp[\beta(\phi_{Fp} - \psi_n)] \tag{4.6b}$$

Note that if we consider ψ_n=0 in the bulk, Equations (4.6a) and (4.6b) then becomes Equations (4.5a) and (4.5b). Surface concentrations of electrons and holes can be obtained by substituting ψ_n with ψ_s in Equations (4.6a) and (4.6b). The derivation of total space-charge density Q_s in the semiconductor under illumination is similar to that at equilibrium. Based on the work of Girisch [39] and Grove [40], Q_s under illumination is given by

$$Q_s = \mp 2qn_i L_{Di} \{F(\psi_s, \phi_{Fp}, \phi_{Fn})\}^{\frac{1}{2}} \tag{4.7}$$

where L_{Di} is the intrinsic Debye length. Note that L_{Di} is different from the extrinsic Debye length L_{Dn} given by Equation (2.21). L_{Di} and function $F(\psi,\phi_{Fp},\phi_{Fn})$ are expressed as

$$L_{Di} \equiv \sqrt{\frac{kT}{q} \times \frac{\varepsilon_s}{2qn_i}} \tag{4.8}$$

$$F(\psi, \phi_{Fp}, \phi_{Fn}) \equiv exp[\beta(\phi_{Fp} - \psi_n)] - exp(\beta \phi_{Fp}) + exp[\beta(\psi_n - \phi_{Fn})] - exp(-\beta \phi_{Fn}) + \beta \psi_n \frac{N_A - N_D}{n_i} \tag{4.9}$$

According to Equation (4.7), Q_s is a function of ψ_s and excess carrier density (which determines ϕ_{Fn} and ϕ_{Fp}). For the MIS structure, the semiconductor bulk is a quasi-neutral region, indicating there is no electric field. From Gauss's law, total charges in the structure should be zero

$$Q_s + Q_f = 0 \tag{4.10}$$

For this structure with certain charges in the insulator, Equation (4.7) is valid under various illumination levels and Q_s can be solved directly for a given ψ_s. However, ψ_s cannot be solved for a given Q_f due to its variation as a function of excess carrier density. We can only use numerical methods to solve for ψ_s from a given Q_s value. A flow chart of the numerical algorithm used in this work is shown in Fig. 4.2. I wrote a Macro script in *Microsoft Excel* to set Q_s to a given value of Q_f by changing the value of ψ_s. After a final ψ_s value determined, n_s and n_p can be calculated from Equation (4.6a).

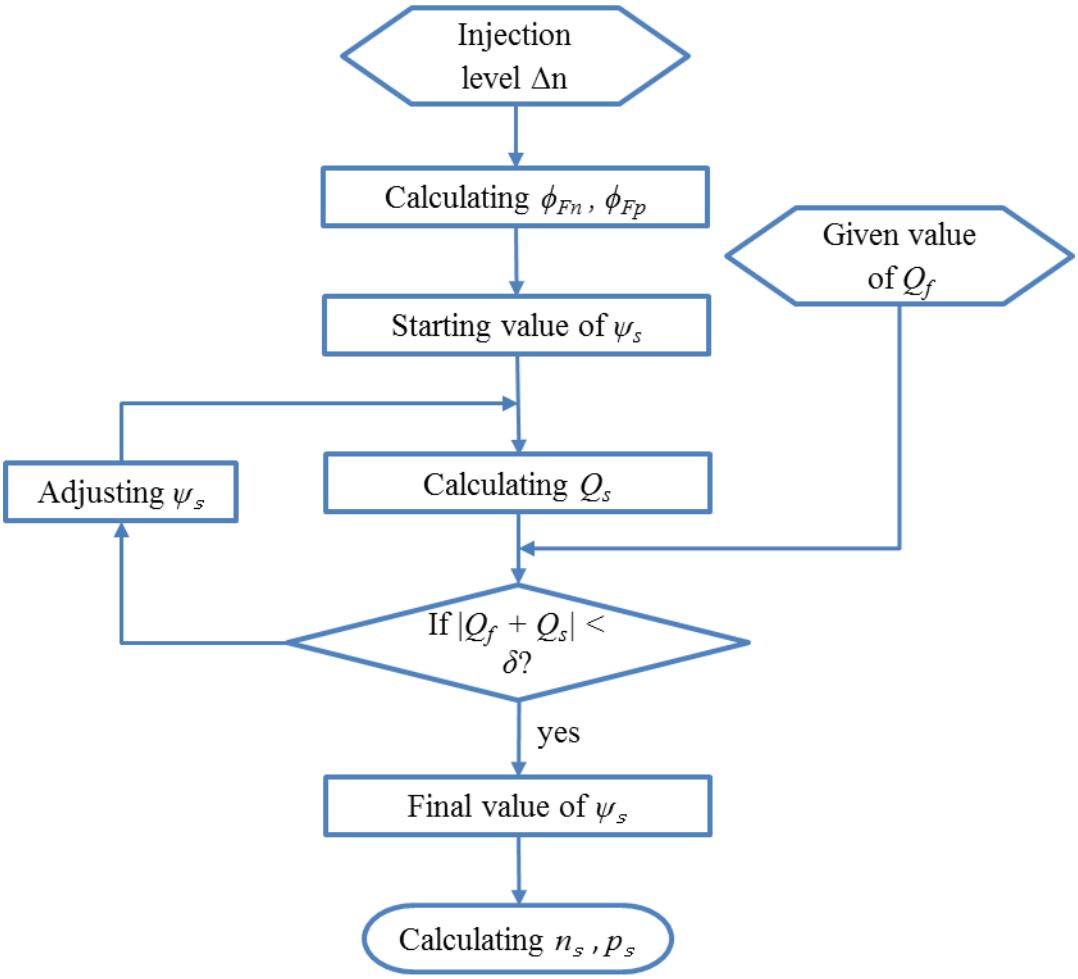

Fig. 4.2. Flowchart of a numerical method for solving for surface potential ψ_s and surface carrier density with insulator charge density Q_f under illumination.

When semiconductor surface is in the strong inversion condition, the surface concentration of holes at equilibrium is significantly higher than the excess carrier density (Δn) under photo-generation. Thus p_s is almost constant under illumination before ultra-high level injection. Fig. 4.3 shows the dependence of p_s and n_s on Δn. p_s is almost constant before the injection level of $1x10^{17}$ cm^{-3},which means the difference between the valence band and the hole quasi-Fermi level is nearly independent of the injection level in that regime. This phenomenon is commonly referred to as the pinning of the hole quasi-Fermi level [41], [42].

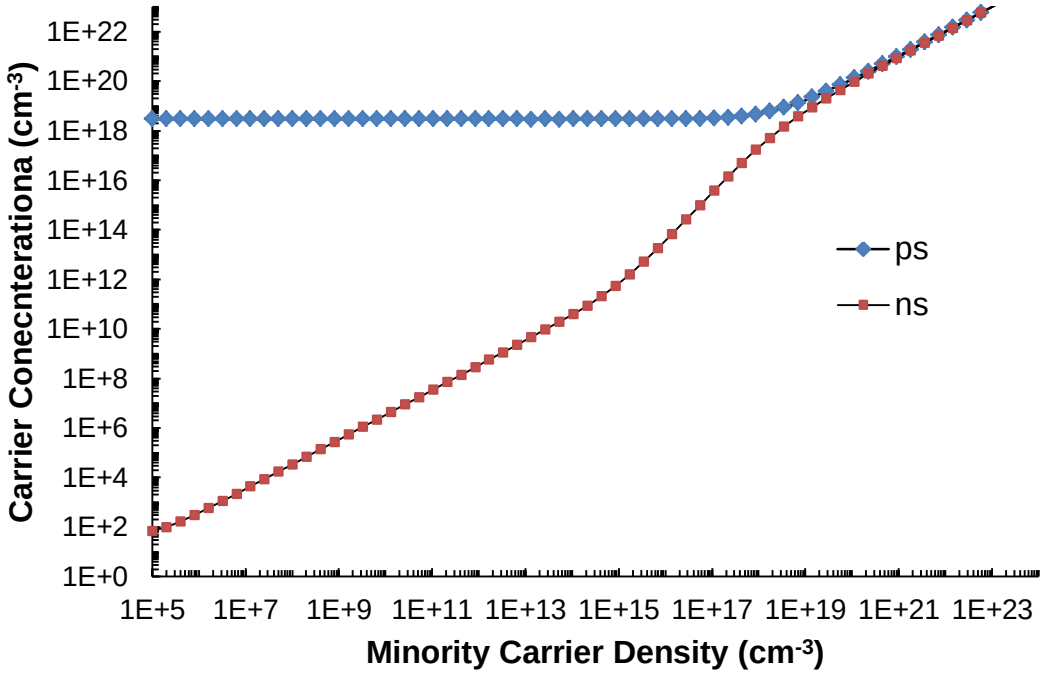

Fig. 4.3. Dependence of surface concentrations of electrons and holes on the injection level, for the n-type Si with doping concentration of $1x10^{15}$ cm^{-3} and insulator charge density of $-1x10^{12}$ cm^{-2}.

4.3 Analytical Simulation

Analytical simulations were performed using parameters in Table 4.1, with the following assumptions: radiative and Auger recombination is neglected; carrier tunneling through Si/SiO_2 interface is neglected. For a specific Q_f value, n_s and p_s were calculated in terms of injection level Δn from the numerical method in Section 4.2. According to Equations (2.27) and (2.34), S_{eff} was then solved. Therefore $1/\tau_{eff}$ was then obtained from Equation (4.3).

Simulation results at flat-band, depletion and inversion are shown in Fig. 4.4. By using the definition of surface conditions from Table 2.2, the behaviors of Auger-corrected inverse lifetime curves are described as:

a) at near flat-band, curves first drop from high levels and then flatten out;

b) at depletion, curves first drop from very high levels, then increase, and flatten out finally;

c) at weak inversion, curve behaviors are very similar to that at depletion, but they flatten out at higher injection levels;

d) at low strong inversion, curves first drop, then increase linearly, and flatten gradually;

e) at high strong inversion, curves are almost linear lines, and the higher $|N_f|$ value give the lower slope as shown in Fig. 4.5.

Table 4.1 Parameters in analytical simulation.

Parameter	**Value**
n-type doping level	1×10^{15} cm^{-3}
Thickness	345 μm
Capture time constant of electrons (τ_{n0})	500 μs
Capture time constant of holes (τ_{p0})	500 μs
Trap energy level (E_t-E_i)	0 eV (single-level at midgap)
Front and rear surface recombination velocity parameters for electrons (S_{n0})	1000 cm/s
Front and rear surface recombination velocity parameters for holes (S_{p0})	1000 cm/s

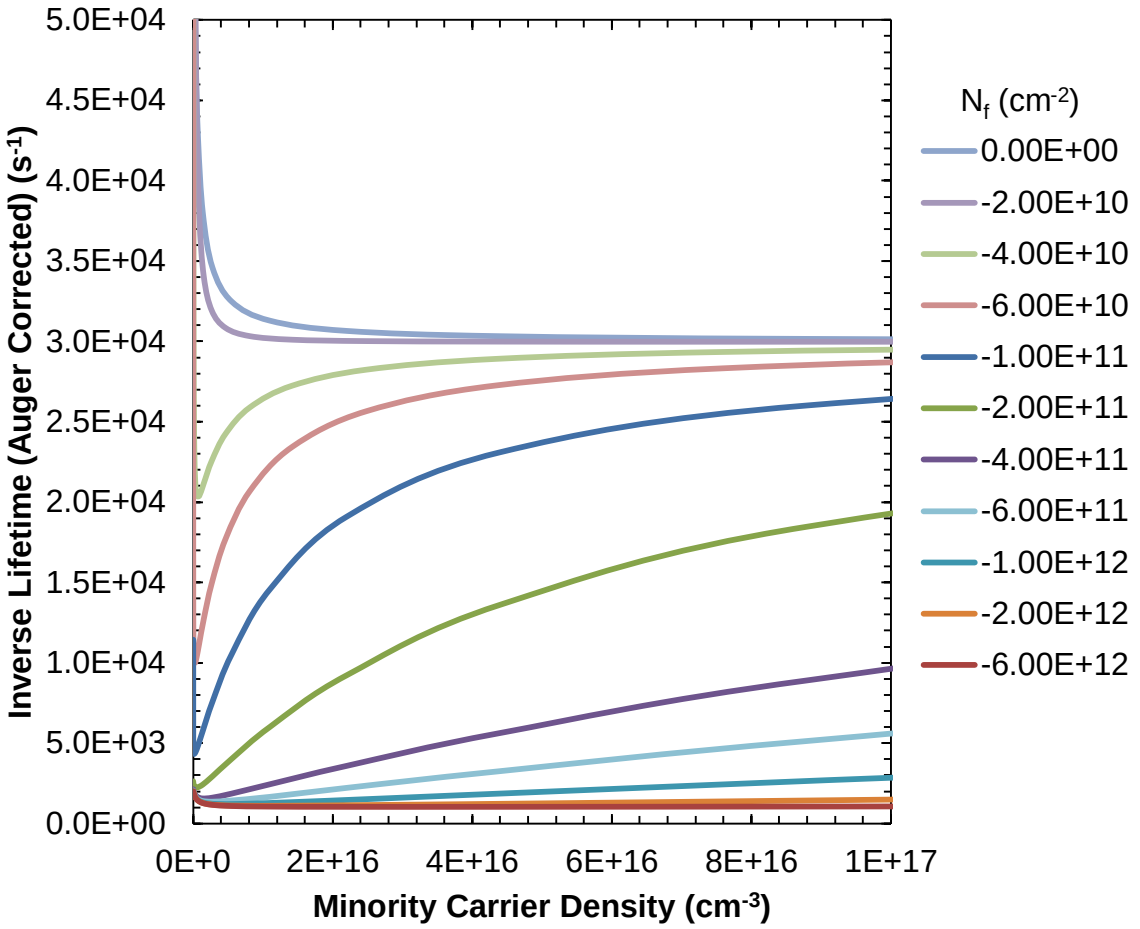

Fig. 4.4. Dependence of simulated inverse lifetime curves on different insulator charge densities with surface at flat-band, depletion and inversion.

Simulation results for the semiconductors with accumulated surfaces are shown in Fig. 4.6. The behaviors of these curves are quite similar to simulations at inversion: curves drop, then increase linearly, and flatten gradually at low accumulation; curves are almost linear lines at high accumulation and the higher $|N_f|$ value give the lower slope.

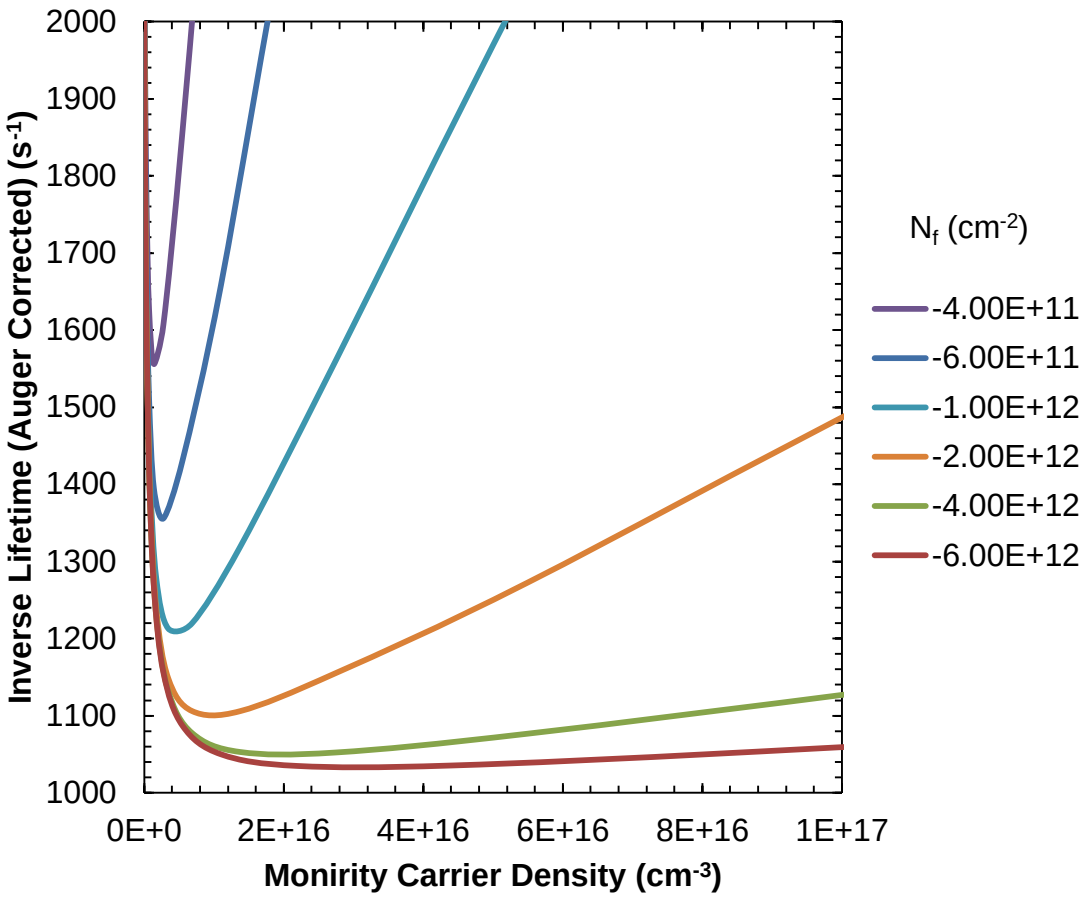

Fig. 4.5. Dependence of simulated inverse lifetime curves on different insulator charge densities with surface at strong inversion.

Simulated inverse lifetime curves at flat-band, depletion and inversion in log-log scale are shown in Fig. 4.7. The different level of injection is defined in Table 4.2. Observations are described below:

a) at ultra-high injection, all curves with various insulator charges end up to the same level;

b) at high injection, curves associated with inverted surfaces increase and have linear regions;

c) at mid-injection, curves slightly decrease due to the injection dependent SRH bulk lifetimes;

d) at low injection, curves show various behaviors depending on surface conditions;

e) at ultra-low injection, curves are flat. $1/\tau_{eff}$ at depletion or weak inversion is higher than it is for the flat-band surface. Highest $1/\tau_{eff}$ occurs when the Fermi-level is at midgap at the surface ($N_f \approx 6x10^{10}$ cm^{-3}).

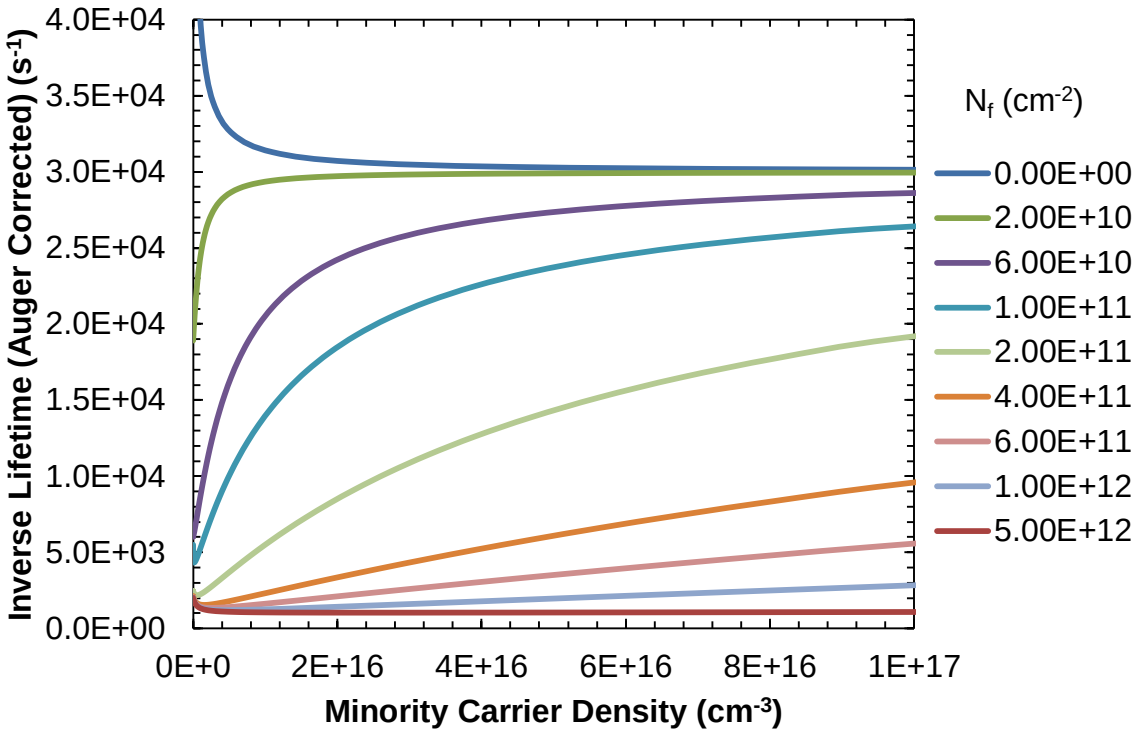

Fig. 4.6. Dependence of simulated inverse lifetime curves on different insulator charge densities with surface at accumulation.

Table 4.2. Definition of injections used in this work for n-type semiconductor. $n_{s,\,eqb}$ and $n_{s,\,eqb}$ are surface concentrations of electron and hole at equilibrium. n_0 is substrate doping concentration.

Level of Injection	Condition
Ultra-high injection	$\Delta n > 10 \times n_{s,\,eqb}\,(or\ p_{s,\,eqb})$
High injection	$\Delta n > 10 \times n_0$
mid-level injection	$\frac{1}{10} n_0 < \Delta n < 10 \times n_0$
Low injection	$\Delta n < \frac{1}{10} n_0$
Ultra-low injection	$\Delta n < \frac{1}{10} p_0$

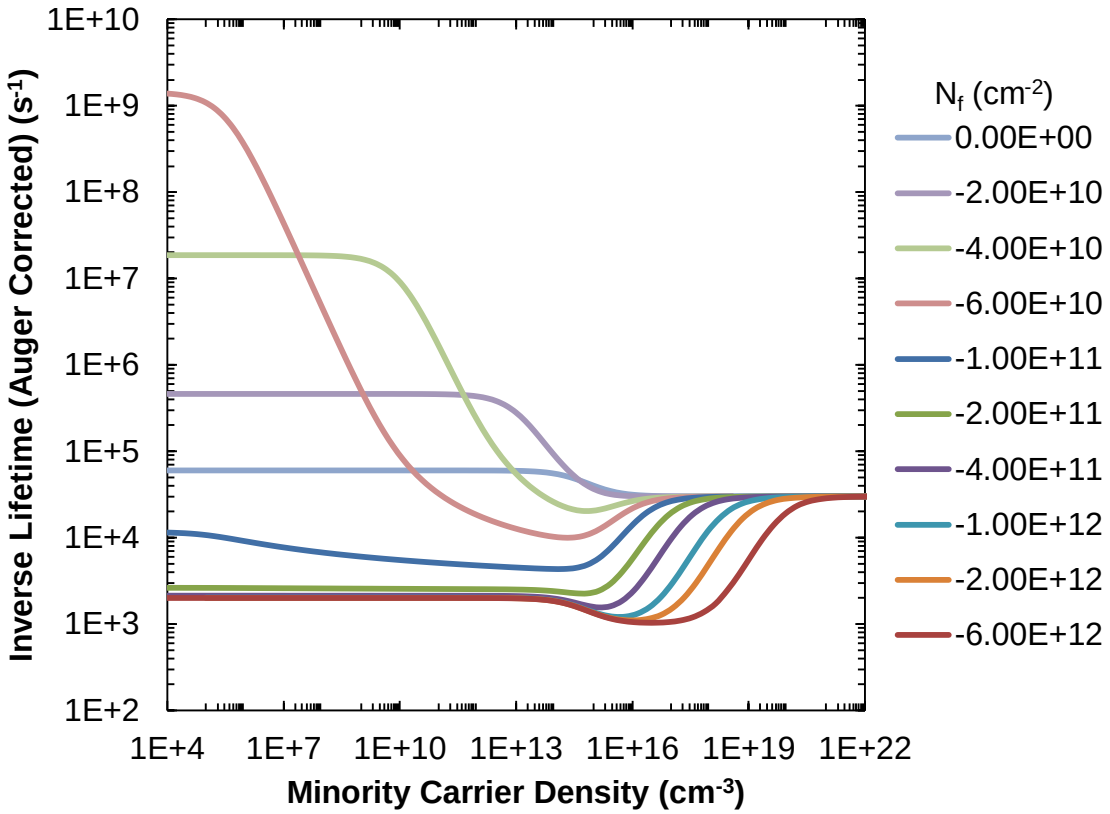

Fig. 4.7. Dependence of simulated inverse lifetime curves on different insulator charge densities with surface at depletion and inversion in log-log scale.

4.4 Explanation of Curves Behaviors and Equation Derivation

4.4.1 Strong inversion condition

The analysis begins with n-type silicon at strong inversion. Under photo-generation with excess carrier concentration Δn, the quasi-fermi levels (QFL) of electron and hole are flat from the bulk to the surface. The product of the electron and hole concentrations (n_s and p_s) at the interface between Si and insulator is expressed as

$$n_s p_s = (n_0 + \Delta n)(p_0 + \Delta n) \tag{4.11}$$

where n_0 and p_0 are the equilibrium concentrations of electrons and holes at the edge of the space charge region.

At high strong inversion, the surface concentration of holes is significantly higher than the photo-generated carriers before ultra-high injection ($p_s >> \Delta n$). Thus, the hole concentration (p_s) at the surface is nearly independent of the injection level and equals to its equilibrium value, by referring to Fig. 4.3. The hole concentration then becomes

$$p_s = p_o \exp\left(-\frac{q\psi_{s,eqb}}{kT}\right) = n_o \exp\left(-\frac{q\psi_{net}}{kT}\right) \tag{4.12}$$

with

$$\psi_{net} = \psi_{s,eqb} - \psi_{inv} \tag{4.13}$$

where $\psi_{s,eqb}$ is the surface band bending at equilibrium, ψ_{inv} is the amount of surface band bending required for hole concentration to be equal to the background doping concentration n_o (referring to Fig. 2.5).

By substituting equation (4.12) into (4.11) and assuming $\Delta n >> p_0$, n_s can be expressed as

$$n_s = \Delta n(1 + \frac{\Delta n}{n_o})exp(\frac{q\psi_{net}}{kT}) \quad (4.14)$$

$p_s >> n_s$ is valid at high strong inversion. The surface recombination rate U_s is described by the classical SRH model. If we assume $p_s >> p_1$ and substitute n_s into surface SRH Equation (2.27), U_s is then calculated as

$$U_s = S_{n0}\Delta n \left(1 + \frac{\Delta n}{n_o}\right) exp(\frac{q\psi_{net}}{kT}) \quad (4.15)$$

Effective lifetime τ_{eff} is determined by bulk lifetime τ_{bulk} and effective surface recombination velocity S_{eff}. For the semiconductor with the same front and rear surface condtions, τ_{eff} can be expressed as by Equation (4.3). Thus the relationship between inverse effective lifetime and excess carrier density is given by

$$\frac{1}{\tau_{eff}} = \frac{1}{\tau_{bulk}} + \frac{2S_{n0}}{W} exp(\frac{q\psi_{net}}{kT}) + \frac{2S_{n0}}{Wn_o} exp(\frac{q\psi_{net}}{kT})\,\Delta n \quad (4.16)$$

Equation (4.16) shows a linear relation between $1/\tau_{eff}$ and Δn. The slope of inverse lifetime curve is determined by both S_{n0} and ψ_{net}. Under low injection, the term $\frac{2S_{n0}}{Wn_o} exp(\frac{q\psi_{net}}{kT})\,\Delta n$ can be neglected due to very small Δn value. Then $1/\tau_{eff}$ is a constant value and the curve is flat. When Δn reaches the background doping concentration, τ_{bulk} increases gradually from a low value ($\tau_{bulk,low}$) to a high value ($\tau_{bulk,high}$). That explains the slight drop for these inverse lifetime curves in that regime. When the injection level is high enough to make the term $\frac{2S_n}{Wn_o} exp(\frac{q\Psi net}{kT})\,\Delta n$ dominant, the curve starts to increase linearly. The slope and y-intercept (y_{int}) of this linear region are given by

$$Slope = \frac{2S_{n0}}{Wn_0} exp\left(\frac{q\psi_{net}}{kT}\right) \quad (4.17)$$

$$y_{int} = \frac{1}{\tau_{bulk}} + \frac{2S_{n0}}{W} exp\left(\frac{q\psi_{net}}{kT}\right) = \frac{1}{\tau_{bulk}} + slope \cdot n_0 \quad (4.18)$$

Note that slope and y_{int} are extracted at high injection, thus τ_{bulk} can be considered as $\tau_{bulk,high}$. From there, ψ_{net} and $\tau_{bulk,high}$ are expressed as

$$\psi_{net} = \frac{kT}{q} ln\left(\frac{Wn_o\, slope}{2S_{n0}}\right) \quad (4.19)$$

$$\tau_{bulk,\, high} = \frac{1}{y_{int} - slope \cdot n_0} \quad (4.20)$$

For a given S_{n0} value, ψ_{net} can be obtained from Equation (4.19), and then Q_s is calculated from Equation (4.7). As $N_f = -Q_s/q$, the insulator charge density N_f can be obtained from this approach.

For the same S_{n0} value, a higher surface charge leads to a larger band bending ψ_{net}, and thus a smaller slope of the curve. Therefore, it provides a fast way to compare surface band bending and charge density of wafers with similar S_{n0}, which is a reasonable assumption for a batch of the same wafers after the same processes.

If we have N_f value extracted from the CV measurement, ψ_{net} can then be determined. Thus from the slope of the inverse lifetime curve, S_{n0} can be determined from this expression

$$S_{n0} = \frac{slope W n_0}{2exp(\frac{q\psi_{net}}{kT})} \quad (4.21)$$

In the lifetime measurement, saturation current density (J_0) can be extracted from the inverse lifetime curve. By comparing Equations (4.2) and (4.16), a linear relationship between slope and J_0 is given by

$$slope = \frac{2J_0}{qn_i^2 W} \tag{4.22}$$

From the above equation, the slope of the linear region in the inverse lifetime curve can be calculated from the J_0 value. Furthermore, Equation (4.21) can be expressed in terms of J_0

$$S_{n0} = \frac{n_o}{qn_i^2} exp\left(-\frac{q\psi_{net}}{kT}\right) J_0 \tag{4.23}$$

4.4.2 Near flat-band condition

A key assumption to make Equation (4.16) valid is that $p_s >> n_s$. As injection level Δn goes up, this assumption will not hold and ends up as $p_s \approx n_s$ at ultra-high injection level. Fig. 4.7 shows all inverse lifetimes end up to the same value under ultra-high level injection. In this case, we have $p_s = n_s = \Delta n$ and the energy bands are flat from the bulk to the surface. Thus the SRV is a constant value given by (2.33) at flat-band. $1/\tau_{eff,\,high}$ is then calculated from Equation (4.3) by substituting S_{eff} with S_{high}

$$\frac{1}{\tau_{eff,\,high}} = \frac{1}{\tau_{bulk,\,high}} + \frac{2}{W} \cdot \frac{S_{p0}}{1 + \frac{S_{p0}}{S_{n0}}} \tag{4.24}$$

Note that $\tau_{bulk,high}$ is the bulk lifetime at high injection, and it is constant. Thus $1/\tau_{eff,high}$ is constant and only depends on surface states (via S_{n0} and S_{p0}) and bulk lifetime.

For samples at high strong inversion and high accumulation, ultra-high injection will not occur below $1x10^{18}$ cm^{-3}. Thus only linear lines can be observed. For wafers in other surface conditions, transitions from linear to flat line or trends of flattening out can be seen.

At ultra-low injection, each of the inverse lifetimes ($1/\tau_{eff,low}$) is constant with specific charge density, according to Fig. 4.7. In this case, $\tau_{bulk,\,low}$ is constant and Δn is

so small that it can be neglected. S_{eff} then becomes a constant. Thus $1/\tau_{eff}$ is a constant according to Equation (4.3). When the Fermi-level is at midgap at the surface, the S_{eff} reaches its maximum (referring to Fig. 2.9), resulting in a highest $1/\tau_{eff}$ value.

Particularly, in the case of flat-band (N_f =0) condition, $1/\tau_{eff,\,low}$ and $1/\tau_{eff,\,high}$ can be derived from Equations (2.31), (2.32) and (4.3). When the trap energy level is at the midgap as in the simulation, we have $n_1=p_1=1x10^{10}$ cm^{-3} << n_0. If τ_{bulk} is very high that $1/\tau_{bulk}$ can be neglected, which is quite common for float-zone (FZ) wafers, and we assume $\sigma_n = \sigma_p$ ($S_{p0}/S_{n0} = 1$), then inverse lifetimes become

$$\frac{1}{\tau_{\text{eff, low}}} = \frac{2S_{\text{p0}}}{W} \tag{4.25}$$

$$\frac{1}{\tau_{\text{eff, high}}} = \frac{S_{\text{p0}}}{W} \tag{4.26}$$

From the above two equations, $1/\tau_{eff,\,high}$ is a half of $1/\tau_{eff,\,low}$, which agrees with the simulation result.

4.4.3 Accumulation condition

The derivation for accumulation condition is similar to that for the strong inversion condition. When the silicon surface is at high accumulation, the concentration of electrons at the silicon surface is significantly higher than the photo-generated carriers ($n_s>>\Delta n$). Thus, n_s is nearly independent of Δn and equals to its equilibrium value. n_s is given by

$$n_s = n_0 \exp\left(\frac{q\psi_{\text{s,eqb}}}{kT}\right) \tag{4.27}$$

By substituting Equation (4.28) into (4.11) and assuming $\Delta n>>p_0$, p_s can be calculated as

$$p_s = \Delta n\left(1+\frac{\Delta n}{n_0}\right) exp\left(-\frac{q\psi_{s,eqb}}{kT}\right) \tag{4.28}$$

At the surface, $n_s >> p_s$ is valid because of high accumulation. If we assume $n_s >> n_1$ and use the relationship in Equation (4.28), the recombination rate becomes

$$U_s = S_p\,\Delta n\,\left(1+\frac{\Delta n}{n_0}\right) exp\left(-\frac{q\psi_{s,eqb}}{kT}\right) \tag{4.29}$$

Substituting Equation (4.29) into (4.3), the inverse lifetime becomes

$$\frac{1}{\tau_{eff}} = \frac{1}{\tau_{bulk}} + \frac{2S_{p0}}{W} exp\left(-\frac{q\psi_{s,eqb}}{kT}\right) + \frac{2S_{p0}}{Wn_0} exp\left(-\frac{q\psi_{s,eqb}}{kT}\right)\Delta n \tag{4.30}$$

Equation (4.30) is analogous to Equation (4.16) for strong inversion condition. Therefore, curve behaviors at accumulation are similar to that at inversion. The conclusion conducted in Section 4.4.1 can be applied to the high accumulation condition as well.

4.4.4 Effect of different SRV parameters

To investigate the effect of SRV parameters (S_{n0} and S_{p0}) on the inverse lifetime curve behavior, simulations with different S_{n0} and S_{p0} (keeping $S_{n0} = S_{p0}$) values are performed, as shown in Fig. 4.8. The shapes of all curves are similar, and the linear to flat line transition always occurs at the same injection level, no matter how S_{n0} and S_{p0} vary. This reveals that the inverse lifetime curve behavior is irrelevant to S_{n0} and S_{p0} values as long as $S_{n0} = S_{p0}$.

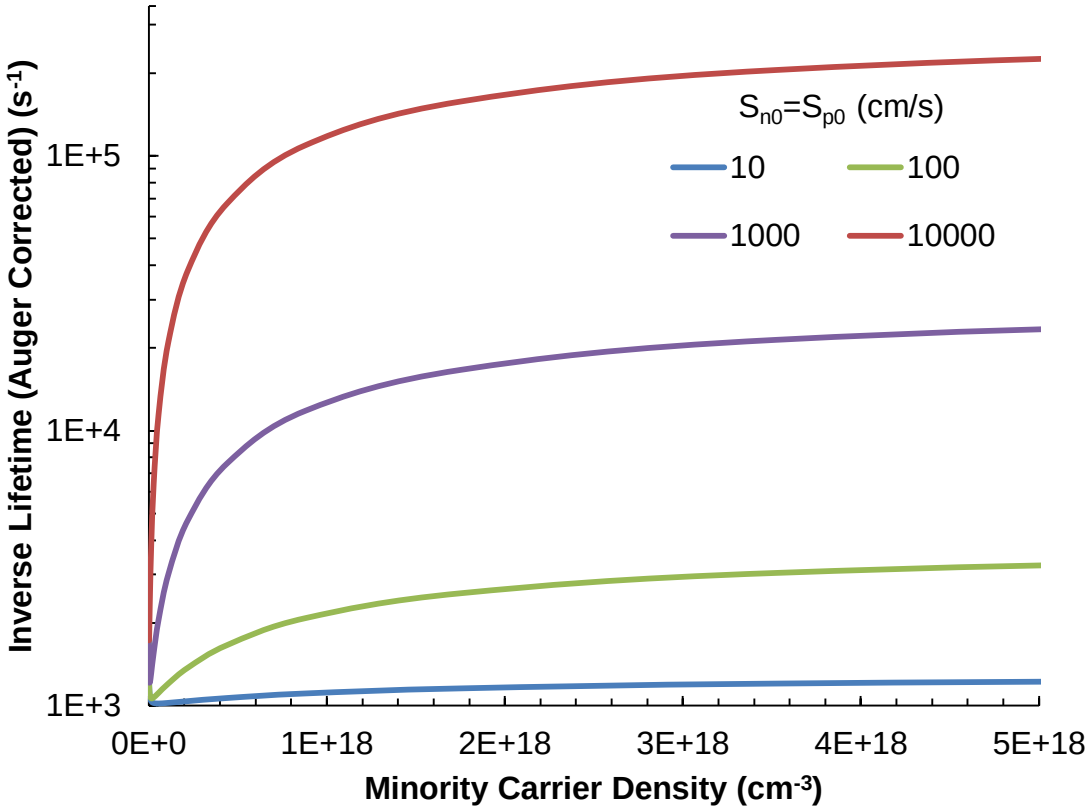

Fig. 4.8. Effect of surface recombination velocity parameters on the inverse lifetime curves. Simulation parameters used are shown in Table 4.1, with insulator charge density of -1×10^{12} cm^{-3} (at high strong inversion).

4.5 Experimental results

Same symmetrical $Si/SiO_2/SiN_x$ stacks in Fig. 3.3 are used in the experiments. Fig. 4.9 shows the experimental inverse lifetime curve after FGA (before any charging experiment). In this situation, insulator charge density should be very small, because FGA can reduce oxide trapped charges and interface state charges. It is observed that the curves drop rapidly at the beginning, and then becomes nearly flat lines (or with slightly negative slope) with increasing injection level. The slightly negative slopes in the flat line region are due to unequal capture cross sections for electrons and holes.

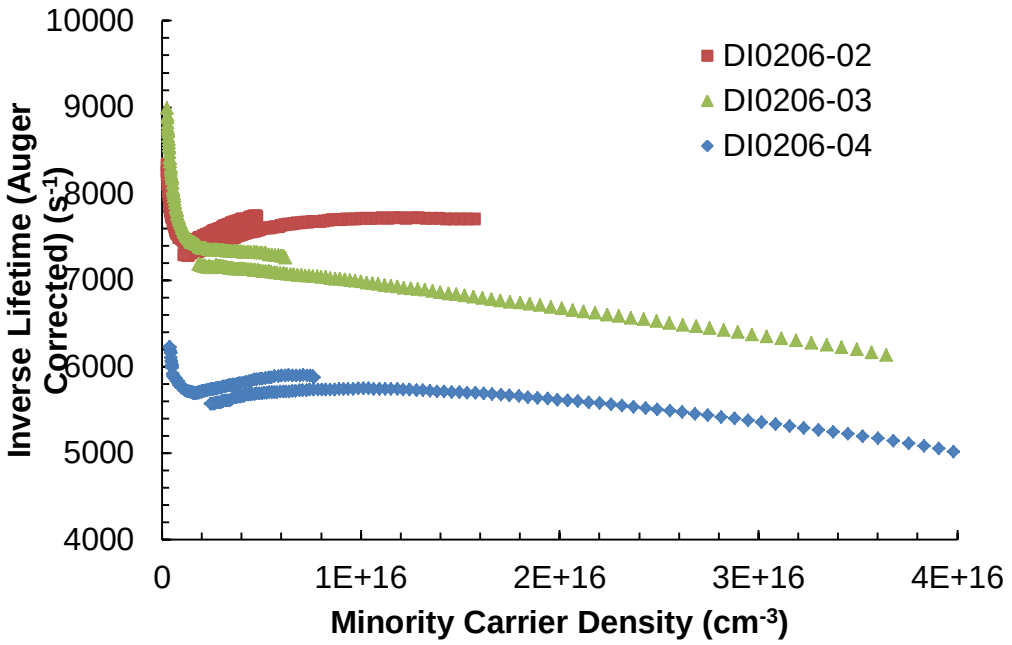

Fig. 4.9. Experimental inverse lifetime curves for samples after FGA (before corona charging).

When positive charges are injected in the SiN_x film, a different behavior of the inverse lifetime curves is observed, as shown in Fig. 4.10. Inverse lifetime curves first drop, then increase linearly for a while, and flattening gradually with increasing injection level. Compared to the simulation results in Fig. 4.4, these samples are most likely in the low accumulation condition. However, the flat-band shifts in their CV measurements are so small that the extracted fixed charge density cannot be trusted.

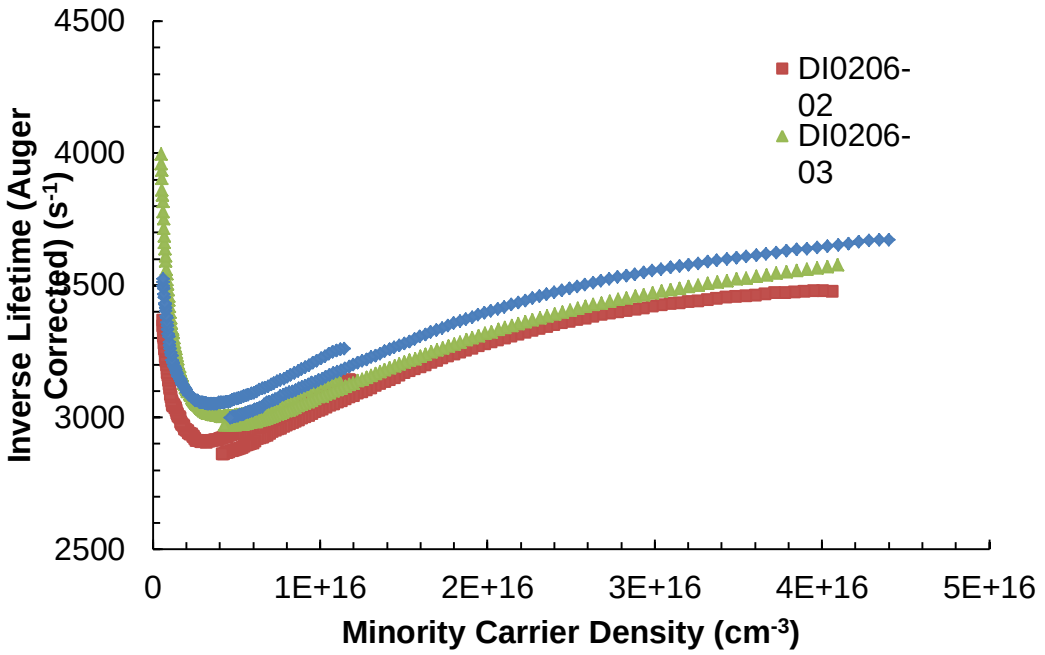

Fig. 4.10. Experimental inverse lifetime curves for samples with positive corona charged insulating films.

When negative charges are injected in SiN_x films, the behavior of inverse lifetime curves is shown in Fig. 4.11. Inverse lifetime curves first drop, then increase linearly. Table 4.3 shows parameters calculated from lifetime measurements. N_f values are the insulator charge densities measured by CV methods and there is no N_f determined for wafer 03 because its CV measurement was out of range. J_0 is extracted from inverse lifetime curve, and the slope of linear line can be calculated via Equation (4.22). According to Table 4.3, the higher charge density leads to the lower slope. S_{n0} can be calculated via Equation (4.21). The calculated S_{n0} values of wafer 01 and 02 are very close, indicating they have similar interface state densities. These two samples are from the same lot with the same fabrication processes, so it makes sense if they have the same surface states densities. Although the calculated S_{n0} should have a large error, this method gave reasonable results. Intercept fit (in unit of μs) is the inverse of y-axis

intercept of the linear fit line, which is the same fit line for extracting J_0 from inverse lifetime curve. τ_{bulk} can be calculated from Equation (4.20). These τ_{bulk} values are close enough to the effective lifetimes of samples after FGA or negative charging as shown in Fig. 3.7. It is likely the calculated τ_{bulk} values are the actual bulks that limit those effective lifetimes. Therefore, this bulk lifetime extraction method is feasible.

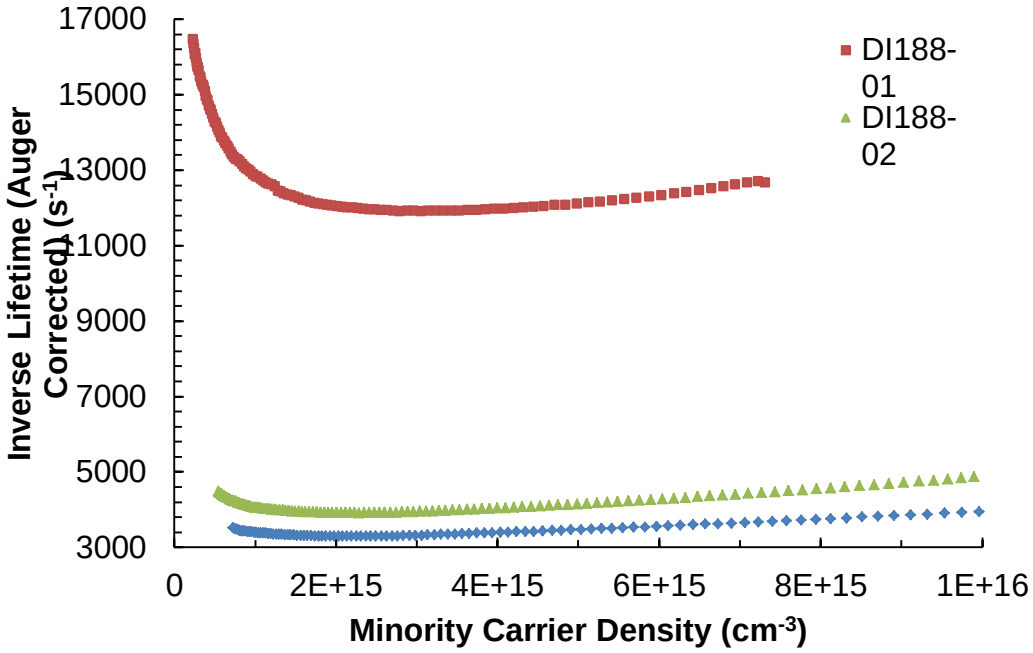

Fig. 4.11. Experimental inverse lifetime curves of samples with negative corona charged insulating films.

Table 4.3. Parameters calculated from lifetime measurement. Experimental J_0 and τ_{bulk} are extracted at MCD $7x10^{15}$ cm^{-3}.

DI0188	**J_0 (fA/cm^2)**	**Slope (cm^3/s)**	**N_f (cm^{-2})**	**ψ_{net} (V)**	**Calculated S_{n0} (cm/s)**	**Intercept fit (µs)**	**$1/\tau_{bulk}$ (s)**	**τ_{bulk} (µs)**
01	109	$1.97x10^{-12}$	$-2.9x10^{12}$	-0.263	$8.93\ x10^5$	95.1	8540	117
02	57	$1.03x10^{-12}$	$-4.2\ x10^{12}$	-0.28	$9.01\ x10^5$	300	2300	435
03	39	$7.07x10^{-13}$	-	-	-	342	2220	451

CHAPTER 5

CONCLUSION & FUTURE WORK

5.1 Conclusion

This work studied field-effect passivation of Si solar cells by charged SiN_x films and a novel insulator characterization method through lifetime measurements. The presence of amphoteric traps (K centers) in the SiN_x layer makes SiN_x an excellent material for field-effect passivation of silicon. Symmetrical $Si/SiO_2/SiN_x$ stacks were developed to study the effect of charges in SiN_x films. The SiO_2 film works as a barrier layer to prevent charge transport between the Si substrate and insulator. In this way, stable charges can be held in the SiN_x film. Positive or negative charges were injected into the SiN_x films by corona charging technique. CV method was used to measure insulator charge density before and after charging. CV results showed the appropriate charging procedure for the corona tool in our lab is: 30s' charging then moving the wafer with an interval of 1 cm from top to bottom then from left to right. Lifetime measurements showed significant improvement of τ_{eff} for either positive or negative charged CZ samples. It is proven that a large amount of charges with either polarity in the overlying insulator is an efficient way to increase the minority carrier lifetime in the CZ silicon, indicating the efficiency enhancement of solar cells.

Based on the mechanism of field-effect passivation, a novel method to determine the insulator charge density (N_f) or SRV parameters was proposed and studied in this work. From simulated inverse lifetime (Auger corrected) vs. minority carrier density

curves, there are different curve behaviors within the Δn regime of $1x10^{14}$ cm^{-3} – $1x10^{17}$ cm^{-3} for different Si surface conditions:

a) at near flat-band, curves first drop from high levels and then flatten out;

b) at depletion, curves first drop from very high levels, then increase, and flatten out finally;

c) at weak inversion, curve behaviors are very similar to that at depletion, but curves flatten out at higher injection levels;

d) at low strong inversion, curves first drop, then increase linearly, and flatten gradually;

e) at high strong inversion, curves are almost linear lines, and the higher $|N_f|$ value give the lower slope;

f) at (low or high) accumulation, curve behaviors are very similar to that at strong inversion.

Those behaviors can be well explained by the theory stated in this work. Therefore, the Si surface condition can be determined from the behavior of the inverse lifetime curve, and then the region of N_f can be calculated. Experiments were performed using samples at near flat-band, high strong inversion and low accumulation. The experimental inverse lifetime curve behaviors corresponded to the simulated curve behaviors.

When the Si surface is at high strong inversion or high accumulation, N_f can be determined from the J_0 value extracted from the lifetime measurement at high injection if SRV parameters (S_{n0} and S_{p0}) are known. If S_{n0} and S_{p0} are unknown, N_f values can be compared from the slopes if we assume all samples have similar S_{n0} and S_{p0} values,

which is a reasonable assumption for a batch of samples with the same substrate under the same processes. If N_f is determined from the CV measurement, S_{n0} or S_{p0} can be calculated from the slope of the inverse lifetime curve. The high injection bulk lifetime (SRH lifetime) is able to be calculated from J_0 and intercept fit, which is also extracted from the lifetime measurement. Therefore, this fast and contactless method through lifetime measurements is proven to be feasible and promising for charged insulator characterization.

5.2 Future Work

Although this novel method is proven to be feasible, it is difficult to extract the accurate value of insulator charge density (N_f) or surface recombination velocity parameters (S_{n0} and S_{p0}). To improve the accuracy, more work needs to be done in the future. S_{n0} and S_{p0} are crucial parameters in this method, because they have significant effect on the shape of the inverse lifetime curve. According to Equation (2.28), S_{n0} and S_{p0} are functions of electron and hole capture cross sections (σ_{n0} and σ_{p0}). Deep-level transient spectroscopy (DLTS) is a measurement to characterize deep defects in the semiconductor. The trap energy level (E_t), σ_{n0} and σ_{p0} can be determined from this measurement. DLTS measurement can be applied to the MIS structures studied in this thesis as well [43].

Investigation on where the linear to flat transition in the inverse lifetime curve occurs for samples at inversion or accumulation is required for accurate characterization. There is a linear region before ultra-high injection in the log-log scale plot for samples at strong inversion. The linear to flat transition point is irrelevant to S_{n0} and S_{p0} values as

long as $S_{n0} = S_{p0}$. More literature study and appropriate equation derivation should be done in the future to understand those phenomena and conduct further analysis.

REFERENCES

[1] U.S. Energy Information Administration. (2011). *Annual Energy Review 2010*, Report number DOE/EIA-0384. Available: http://www.eia.gov/totalenergy/data/annual/pdf/aer.pdf

[2] National Oceanic and Atmospheric Administration, National Climatic Data Center. (2010, July). *State of the Climate in 2009*. Available: http://www.ncdc.noaa.gov/bams-state-of-the-climate/2009.php

[3] German Advisory Council on Global Change. (2003). *World in Transition - Towards Sustainable Energy Systems*. Available: http://www.wbgu.de/wbgu_jg2003_kurz_engl.html

[4] European Commission Joint Research Centre. (2013, Sep 30). *PV Production Grows Despite a Crisis-Driven Decline in Investment*. Available: http://phys.org/news/2013-09-pv-production-crisis-driven-decline-investment.html

[5] US Department of Energy. (2011, Nov). *2010 Solar Technologies Market Report*. Available: http://www.nrel.gov/docs/fy12osti/51847.pdf

[6] S. Y. Herasimenka, C. J. Tracy, V. Sharma, N. Vulic, W. J. Dauksher, and S. G., Bowden, "Surface passivation of n-type c-Si wafers by a-Si/SiO_2/SiN_x stack with< 1 cm/s effective surface recombination velocity," *Applied Physics Letters*, vol. 103, no. 18, pp. 183903, 2013.

[7] G. Agostinelli, A. Delabie, P. Vitanov, Z. Alexieva, H. F. W. Dekkers, S. De Wolf, and G. Beaucarne, "Very low surface recombination velocities on p-type silicon wafers passivated with a dielectric with fixed negative charge," *Solar Energy Materials and Solar Cells*, vol. 90, no. 18, 3438-3443, 2006.

[8] C. Honsberg and S. Bowden. (2014). *PVCDROM*. Available: http://www.pveducation.org/pvcdrom

[9] H. Schlangenotto, H Meader, and W. Gerlach, "Temperature dependence of the radiative recombination coefficient in silicon," *Physica Status Solidi (A)*, 21, pp. 357, 1974.

[10] J. Dziewior and W. Schmid, "Auger coefficients for highly doped and highly excited silicon," *Applied Physics Letters*, 31, pp. 346-348, 1977.

[11] W. Shockley and W. T. Read, "Statistics of the recombinations of holes and electrons," *Physical Review*, vol.87, pp. 835-842, 1952.

[12] R. N. Hall, "Electron-hole recombination in germanium," *Physical Review*, vol. 87, pp. 387-387, 1952.

[13] Recombination Calculator, PV Lighthouse. (2014). Available: http://www.pvlighthouse.com.au/calculators/recombination%20calculator/recombination%20calculator.aspx

[14] S. M. Sze and K. K. Ng, *Physics of semiconductor devices*. Hoboken, NJ: John Wiley & Sons. 2006.

[15] E. Robert, "Evacuation dynamics: Empirical results, modeling and applications," Ph.D. Dissertation, Technischen Universität Wien, 2007.

[16] A. G. Aberle, *Crystalline silicon solar cells: advanced surface passivation and analysis*. Sydney, Australia: Centre for Photovoltaic Engineering. University of New South Wales, 1999.

[17] M. A. Green, *Silicon solar cells: advanced principles & practice*. Sydney, Australia: Centre for Photovoltaic Devices and Systems, University of New South Wales, 1995.

[18] D. K. Schroder, *Semiconductor material and device characterization*. Hoboken, NJ: John Wiley & Sons. 2006.

[19] E. H. Nicollian and J. R. Brews, *MOS (Metal Oxide Semiconductor) physics and Technology*, New York, NY: Wiley, 1982.

[20] D. Frohman-Bentchkowsky, "The metal-nitride-oxide-silicon (MNOS) transistor—characteristics and applications," *Proceedings of the IEEE*, vol. 58, no. 8, pp. 1207-1219, 1970.

[21] D. Frohman-Bentchkowsky, and M. Lenzlinger, "Charge Transport and Storage in Metal‐Nitride‐Oxide‐Silicon (MNOS) Structures," *Journal of Applied Physics*, vol. 40, no. 8, pp. 3307-3319, 2003.

[22] K.I. Lundstrom and C.M. Svensson, "Properties of MNOS structures," *IEEE Transactions on Electron Devices*, vol. 19, pp. 826–836, 1972.

[23] S. Yokoyama, M. Hirose, Y. Osaka, "Electron Spin Resonance in Discharge-Produced Silicon Nitride," *Japanese Journal of Applied Physics*, vol. 20, issue 1, pp. L35–L37, 1981.

[24] D.T. Krick, P.M. Lenahan, J. Kanicki, "Stable photoinduced paramagnetic defects in hydrogenated amorphous silicon nitride," *Applied Physics Letters*, vol. 51, pp. 608-610, 1987.

[25] D.T. Krick, P.M. Lenahan, J. Kanicki, "Nature of the dominant deep trap in amorphous silicon nitride," *Physical Review B*, vol. 38, pp. 8226–8229, 1988

[26] W. L. Warren, and P. M. Lenahan, "Electron-nuclear double-resonance and electron-spin-resonance study of silicon dangling-bond centers in silicon nitride," *Physical Review B*, vol. 42, no.3, 1773, 1990.

[27] W. L. Warren, F. C. Rong, E. H. Poindexter, G. J. Gerardi, & J. Kanicki, "Structural identification of the silicon and nitrogen dangling-bond centers in amorphous silicon nitride," *Journal of applied physics*, vol. 70, no. 1, pp. 346-354, 1991.

[28] W. L. Warren, C. H. Seager, J. Kanicki, M. S. Crowder, and E. Sigari. "Ultraviolet light induced annihilation of silicon dangling bonds in hydrogenated amorphous silicon nitride films." *Journal of applied physics*, vol. 77, no. 11, pp. 5730-5735, 1995.

[29] V. Sharma, "Study of Charges Present in Silicon Nitride Thin Films and Their Effect on Silicon Solar Cell Efficiencies." PhD dissertation, Arizona State University, 2013.

[30] W. L. Warren, J. Kanicki, F. C. Rong, and E. H. Poindexter, "Paramagnetic Point Defects in Amorphous Silicon Dioxide and Amorphous Silicon Nitride Thin Films II," *Journal of the Electrochemical Society*, vol. 139, no. 3, 880-889, 1992.

[31] G. A. Corker, & C. M. Svensson, "Sodium‐Induced Work Function Shift of Mercury as a Metal‐Oxide‐Semiconductor Electrode," *Journal of The Electrochemical Society*, vol. 125, no. 11, pp. 1881-1883, 1978.

[32] D. K. Schroder, "Surface voltage and surface photovoltage: history, theory and applications," *Measurement Science and Technology*, vol. 12, no. 3, pp. R16, 2001.

[33] *WCT-120 Photoconductance Lifetime Tester and Optional Suns–Voc User Manual*. Sinton Instruments, Boulder, CO, 2012.

[34] R. A. Sinton, A. Cuevas, and M. Stuckings, "Quasi-steady-state photoconductance, a new method for solar cell material and device characterization," in *Photovoltaic Specialists Conference, Conference Record of the Twenty Fifth IEEE*, pp. 457-460, 1996.

[35] D.E. Kane and R.M. Swanson, "Measurement of the emitter saturation current by a contactless photoconductivity decay method," *Proceedings 18th IEEE Photovoltaic Specialists Conference*, pp. 578–583, 1985.

[36] H. Nagel, C. Berge, and A. G. Aberle, "Generalized analysis of quasi-steady-state and quasi-transient measurements of carrier lifetimes in semiconductors," *Journal of Applied Physics*, vol. 86, no. 11, pp. 6218–6221, 1999.

[37] V. Sharma, C. Tracy, D. Schroder, S. Herasimenka, W. Dauksher, and S. Bowden, "Manipulation of K center charge states in silicon nitride films to achieve excellent surface passivation for silicon solar cells," *Applied Physics Letters*, vol. 104, no. 5, 053503, 2014.

[38] H. Mäckel, and K. Varner, "On the determination of the emitter saturation current density from lifetime measurements of silicon devices," *Progress in Photovoltaics: Research and Applications*, vol. 21, no. 5, pp. 850-866, 2013.

[39] R. B. Girisch, R. P. Mertens, and R. F. De Keersmaecker. Determination of Si-SiO 2 interface recombination parameters using a gate-controlled point-junction diode under illumination. *Electron Devices, IEEE Transactions on*, vol. 35, no. 2, pp. 203-222, 1988.

[40] A. S. Grove, and D. J. Fitzgerald, "Surface effects on< i> p</i>-< i> n</i> junctions: Characteristics of surface space-charge regions under non-equilibrium conditions," *Solid-State Electronics*, vol. 9, no. 8, pp. 783-806, 1966.

[41] E. Yablonovitch, & T. J. Gmitter, "A contactless minority lifetime probe of heterostructures, surfaces, interfaces and bulk wafers," *Solid-state electronics*, vol. 35. no. 3, pp. 261-267, 1992.

[42] M. A. Green, and R. B. Godfrey, "MIS solar cell-General theory and new experimental results for silicon," *Applied Physics Letters*, vol. 29, no. 9, pp. 610-612, 2008.

[43] M. Schulz and E. Klausmann, "Transient capacitance measurements of interface states on the intentionally contaminated Si-SiO_2 interface," *Applied physics*, vol. 18, no. 2, pp. 169-175, 1979.